Electronic Supplementary Material (ESI) for ChemComm.
This journal is © The Royal Society of Chemistry 2023

Supporting Information for Manuscript

Amine-Modified Polyionic Liquid Supports Enhance the Efficacy of PdNPs for the Catalytic Hydrogenation of CO_2 to Formate

Reece Paterson, Luke E. Fahy, Elisabetta Arca,* Casey Dixon, Corinne Y. Wills, Han Yan, Anthony Griffths, Sean M. Collins, Kejun Wu, Richard A. Bourne, Thomas W. Chamberlain,* Julian G. Knight, Simon Doherty*

Contents

General Comments

All reagents were purchased from commercial suppliers and used without further purification. Monomer (4-vinylphenyl)methanamine was prepared as previously described.[1] Polymer ^{1}H NMR spectra were recorded in methanol-d_4 on a Bruker Avance II 400 NMR spectrometer, operating at 399.78 MHz. For more accurate peak integrals, ^{1}H NMR spectra of CO_2 hydrogenation products were recorded on a Bruker Avance III 300 NMR spectrometer, operating at 300.13 MHz, with an 80 s relaxation delay; 50 µL of D_2O was added to samples for locking and non-deuterated dimethylsulfoxide was used as an internal standard. All chemical shifts are quoted in ppm relative to tetramethylsilane (^{1}H, ^{13}C) and nitromethane (^{15}N). Solid-state ^{13}C MAS NMR and ^{15}N MAS NMR spectra were recorded at 125.78 and 50.68 MHz, respectively, using a Bruker Avance III HD 500 NMR spectrometer with 4 mm rotors. They were obtained using cross-polarisation (^{13}C and ^{15}N) and sideband suppression (^{13}C) with a 5-10 s relaxation delay, 1.2-2.3 ms (^{13}C) or 1.7-2.3 ms (^{15}N) contact time at ambient probe temperature (~25 °C) and at a MAS rate of 10 kHz. Spectral referencing was with respect to an external sample of neat tetramethylsilane (carried out by setting the high-frequency signal from adamantane to 37.8 ppm). SEM images were acquired on a Tescan Vega 3LMU scanning electron microscope with digital image collection. XPS analysis was conducted using a Kratos Axis Ultra DLD (Kratos, Harwell, UK) with a monochromatic Al Kα (λ =1486.7 eV) X-ray source operated at 225 W. The analysis chamber base-pressure was better than $1x10^{-8}$ mbar. Samples were mounted using double-sided carbon tape for polymers and $PdCl_4$ precatalysts, and copper tape for PdNP samples isolated post-catalysis. Surface charge compensation was performed using a low energy electron flood gun. Initial survey spectra were recorded at a pass energy of 80 eV, using a step size of 0.5 eV, with a scan range between 0 – 1400 eV. High resolution spectra were then collected for individual elements at a pass energy of 20 eV, using a step size of 0.1 eV. The data presented has not been rescaled with respect to any internal or

external reference, instead interpretation relied on the comparison of binding energy separations.[2] Data analysis was performed using Igor Pro software with a custom-written program from Schmid et al.[3] Curves were fitted using a Gaussian/Lorentzian peak shape with a ratio of 70:30 and backgrounds were subtracted using a Shirley algorithm. Pd 3d core levels were fit using a spin-orbit doublet separation of 5.3 eV and an area ratio of 3:2 between $3d_{5/2}$ and $3d_{3/2}$ components. Metallic Pd 3d signals were fit using an asymmetric Gaussian-Lorentzian line shape, similar to asymmetric pseudo-Voigt profiles previously reported for Pd 3d and Pt 4f.[3] Cl 2p signals were fit as doublets with $2p_{3/2}$ and $2p_{1/2}$ components constrained to a peak area ratio of 1:2 and a doublet separation of 1.6 eV. Samples for transmission electron microscopy (TEM) were dispersed in ethanol using an ultrasonic bath and deposited on lacey carbon film coated copper grids. TEM images were acquired on a FEI Tecnai TF20 field emission gun microscope operating at 200 kV. NP size distribution histograms were obtained from measurements of at least 100 different NPs assuming a spherical shape and with random distribution. The palladium loadings were quantified using inductively coupled plasma optical emission spectroscopy (ICP-OES) on an Agilent 5800 ICP-OES instrument. For digestion, samples were ashed using a propane torch before stirring overnight in aqua regia (3:1, $HCl:HNO_3$). FT-IR spectroscopy was performed on a Varian 800 FT-IR instrument (Varian Inc.).

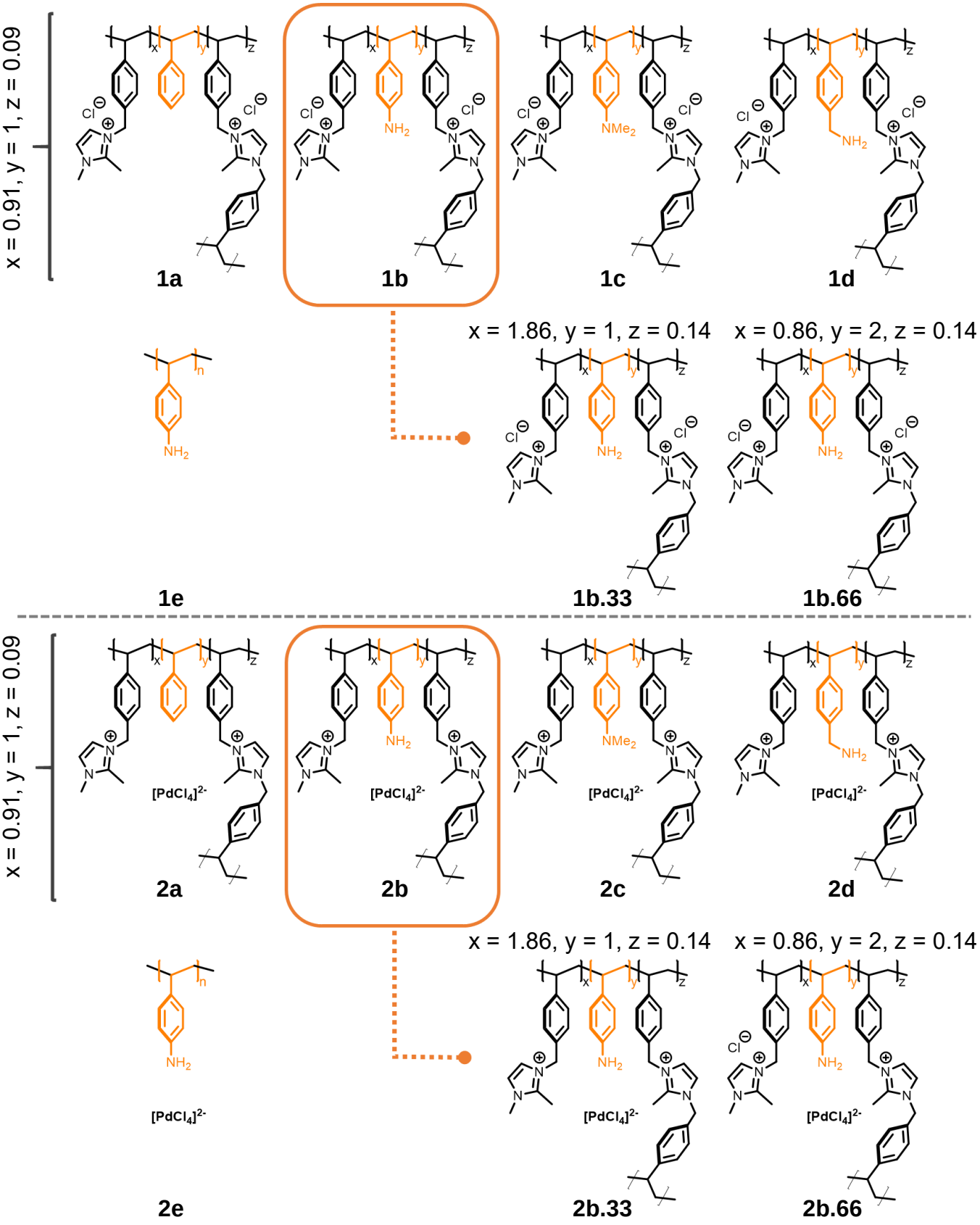

Figure S1 Structures of functionalised PIIL polymers **1a-e** and their corresponding $[PdCl_4]^{2-}$ loaded precatalysts **2a-e**.

Experimental

Synthesis of *N,N*-Dimethyl-4-vinylaniline

In an oven-dried Schlenk flask under N_2, n-butyl lithium (2.5 M in hexane, 13.4 mL, 33.5 mmol) was added dropwise to a stirring solution of methyltriphenylphosphonium bromide (12.0 g, 33.5 mmol) in anhydrous tetrahydrofuran (100 mL). The reaction mixture was allowed to stir for 15 minutes at room temperature, affording an orange solution. After this time, 4-(dimethylamino)benzaldehyde (5.0 g, 33.5 mmol) was added dropwise before stirring the solution at room temperature forming a pale yellow. After 2 hours, the mixture was quenched with saturated ammonium chloride solution and the product was extracted with dichloromethane (4 x 30 mL). The solvent was reduced under *vacuo* before purifying the crude product by column chromatography (10:90 ethyl acetate/petroleum ether). The organic fractions were collected, dried over magnesium sulphate, and filtered before reducing the solvent under *vacuo* to afford a yellow oil in 46% yield. ^{1}H NMR (400 MHz, $CDCl_3$) δ 7.32 (d, J = 8.9 Hz, 2H), 6.70 (d, J = 8.9 Hz, 2H), 6.65 (dd, J = 16.0, 12.0 Hz, 1H), 5.55 (d, J = 17.6 Hz, 1H), 5.03 (d, J = 11.0 Hz, 1H), 2.97 (s, 6H). ^{13}C NMR (300 MHz, $CDCl_3$) δ 150.36, 136.71, 127.26, 126.30, 112.43, 109.45, 40.63.

General Procedure for Synthesis of Functionalised Polymer Immobilized Ionic Liquid Supports 1-d.

A screw-top Schlenk flask was charged with 1,2-dimethyl-3-(4-vinylbenzyl)-imidazolium chloride (18.1 mmol), styrene or amine-modified styrene monomer (19.9 mmol), 2-methyl-1,3-bis(4-vinylbenzyl)-imidazolium chloride (1.8 mmol) and ethanol (corresponding to an ionic liquid : amine : crosslinker ratio of 0.91:1:0.09). Upon complete dissolution, the mixture was charged with azobis(2-methylpropionitrile) (5 mol%), before immediately degassing the solution *via* the freeze-thaw technique (6 cycles). The mixture was then stirred and heated at

80 °C. After 96 hours, the flask was charged with an additional portion of azobis(2-methylpropionitrile) (5 mol%), before degassing and stirring for a further 24 hours at 80 °C. After this time, the flask was allowed to cool to room temperature before precipitating the polymer by dropwise addition to stirring diethyl ether. The resulting precipitate was isolated by filtration, washed with diethyl ether, and dried under *vacuo* to afford an off-white/yellow powder. The same procedure was repeated for the preparation of polymers **1b.33** and **1b.66**, though with an ionic liquid : amine : crosslinker ratio of 1.86:1:0.14 and 0.86:2:0.14 respectively.

Synthesis of Poly-(4-amino)-styrene (1e).

A screw-top Schlenk flask was charged with 4-vinylaniline (11.0 mmol) and ethanol (20 mL) and after complete dissolution azobis(2-methylpropionitrile) (5 mol%) was added. The contents of the flask were degassed *via* the freeze-thaw technique (6 cycles). The mixture was then stirred and heated at 80 °C. After 72 hours, the flask was cooled to room temperature before precipitating the polymer by dropwise addition to stirring diethyl ether. The resulting precipitate was isolated by filtration, washed with diethyl ether, and dried under *vacuo* to afford a pale-yellow powder.

General Procedure for Generation of $PdCl_4$-Loaded Functionalised Polymer Immobilized Ionic Liquid Precatalysts.

For **2a-d** and **2b.66**, a round-bottomed flask charged with palladium dichloride (4.2 mmol), NaCl (92.4 mmol) and water (20 mL) was heated to 80 °C for *ca*. 40 min to afford a clear red solution. A solution of the corresponding polymer **1a-d** or **1b.66** (8.4 mmol) in ethanol (20 mL) was subsequently added in one portion, and the resulting mixture allowed to stir overnight at room temperature, during which time a brick-red precipitate formed. A pale orange/yellow

solid was isolated from the suspension *via* centrifugation which was washed with deionized water (4 x 40 mL), ethanol (4 x 40 mL) and diethyl ether (2 x 20 mL) and dried under *vacuo* to afford a fine orange powder. The same procedure was repeated for the preparation of precatalyst **2b.33**, with 4.2 mmol of polymer **1b.33** (Pd : polymer ratio of 1 : 1).

Synthesis of $PdCl_4$-Loaded Poly-(4-amino)-styrene (2e).

A round-bottom flask charged with NaCl (92.4 mmol) deionized water (20 mL) and $PdCl_2$ (4.2 mmol) and the mixture stirred at 80 ^oC. Upon the formation of a clear red solution, poly-(4-amino)-styrene (4.2 mmol) dissolved in ethanol (10 mL) was added in one portion, and the resulting mixture allowed to stir overnight at room temperature, during which time a brick-red precipitate formed. A pale orange solid was isolated from the suspension *via* centrifugation, washed with deionized water (4 x 40 mL), ethanol (4 x 40 mL) and diethyl ether (2 x 20 mL) and dried under *vacuo* to afford a fine orange powder.

General Procedure for the Thermal Hydrogenation of CO_2

A stainless-steel autoclave was charged with precatalyst **2a-e** (6 μmol Pd) and an aqueous solution of base (20 mL, 0.65 M). The autoclave was sealed and purged with a 1:1 mixture of H_2 : CO_2 gas (5 cycles), before pressurising to 40 bar at room temperature. The vessel was then heated to 100 ^oC and stirred mechanically for 2 hours. After this time, the autoclave was allowed to cool to room temperature before venting the gas. Dimethylsulfoxide was added to the resulting solution as an internal standard, and the product mixture was analysed by ^1H NMR spectroscopy.

ICP-OES Results

Table S1 Palladium loadings of precatalysts **2a-e**, as determined by ICP-OES.

Precatalyst	wt%Pd	Loading of Pd (mmol·g^{-1})
2a	10.44	0.98
2b	11.66	1.10
2c	8.45	0.79
2d	9.75	0.92
2b.33	13.15	1.24
2b.66	8.14	0.76
2e	3.83	0.36

Reaction Optimisation

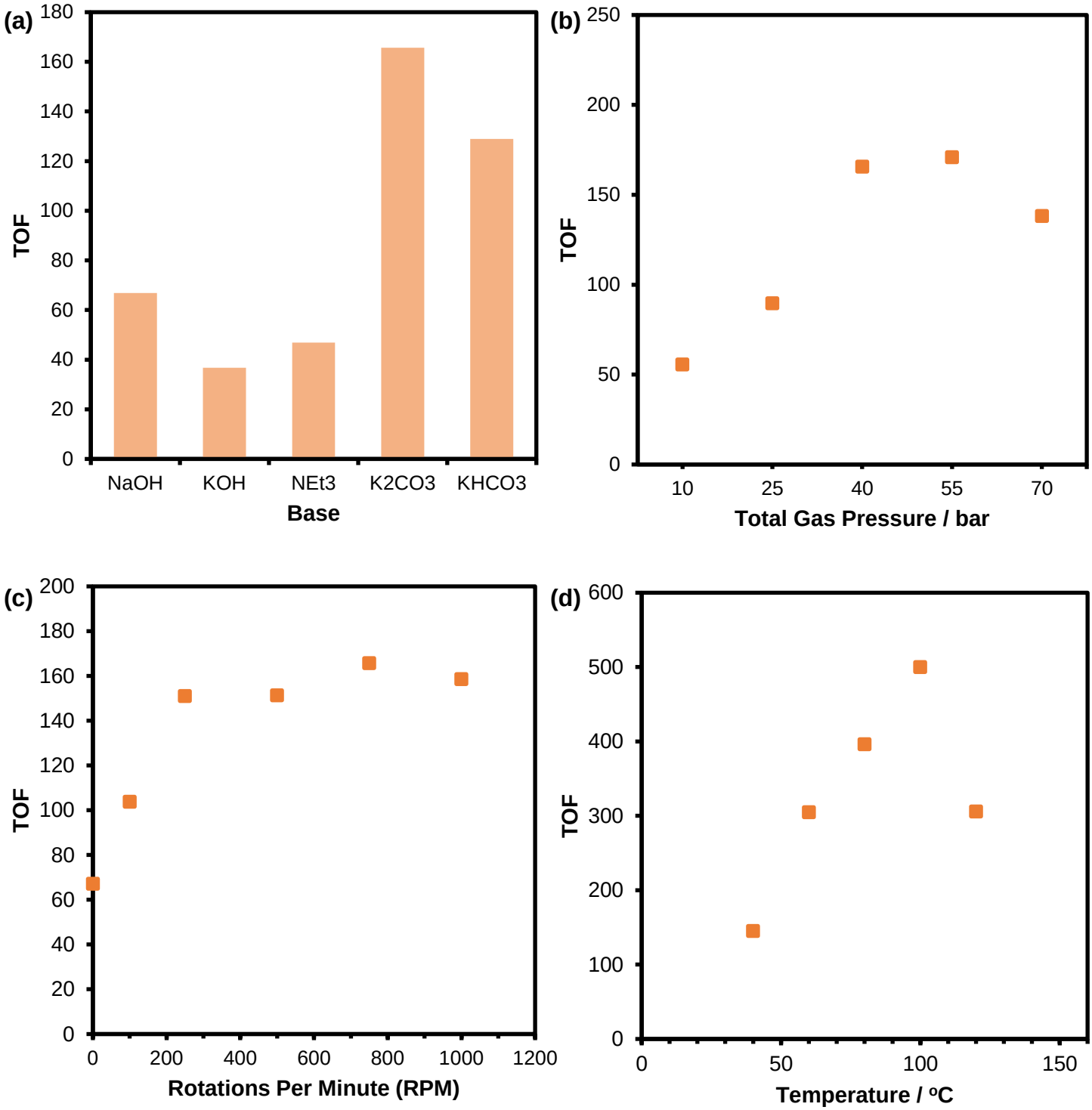

Figure S2 (a) Screening of various bases for the hydrogenation of CO_2, catalysed by **2a** (6 µmol Pd), at 100 ºC with 40 bar of reactive gas. (b) Screening of total gas pressure (1:1 mixture of H_2 : CO_2), catalysed by **2a** (6 µmol Pd), at 100 ºC. (c) Screening of stirring speed for the hydrogenation of CO_2 catalysed by **2a** (6 µmol Pd), at 100 ºC with 40 bar of reactive gas. (d) Screening of reaction temperature for the hydrogenation of CO_2 catalysed by **2b.66** (6 µmol Pd), with 40 bar of reactive gas.

Reaction Time Profile

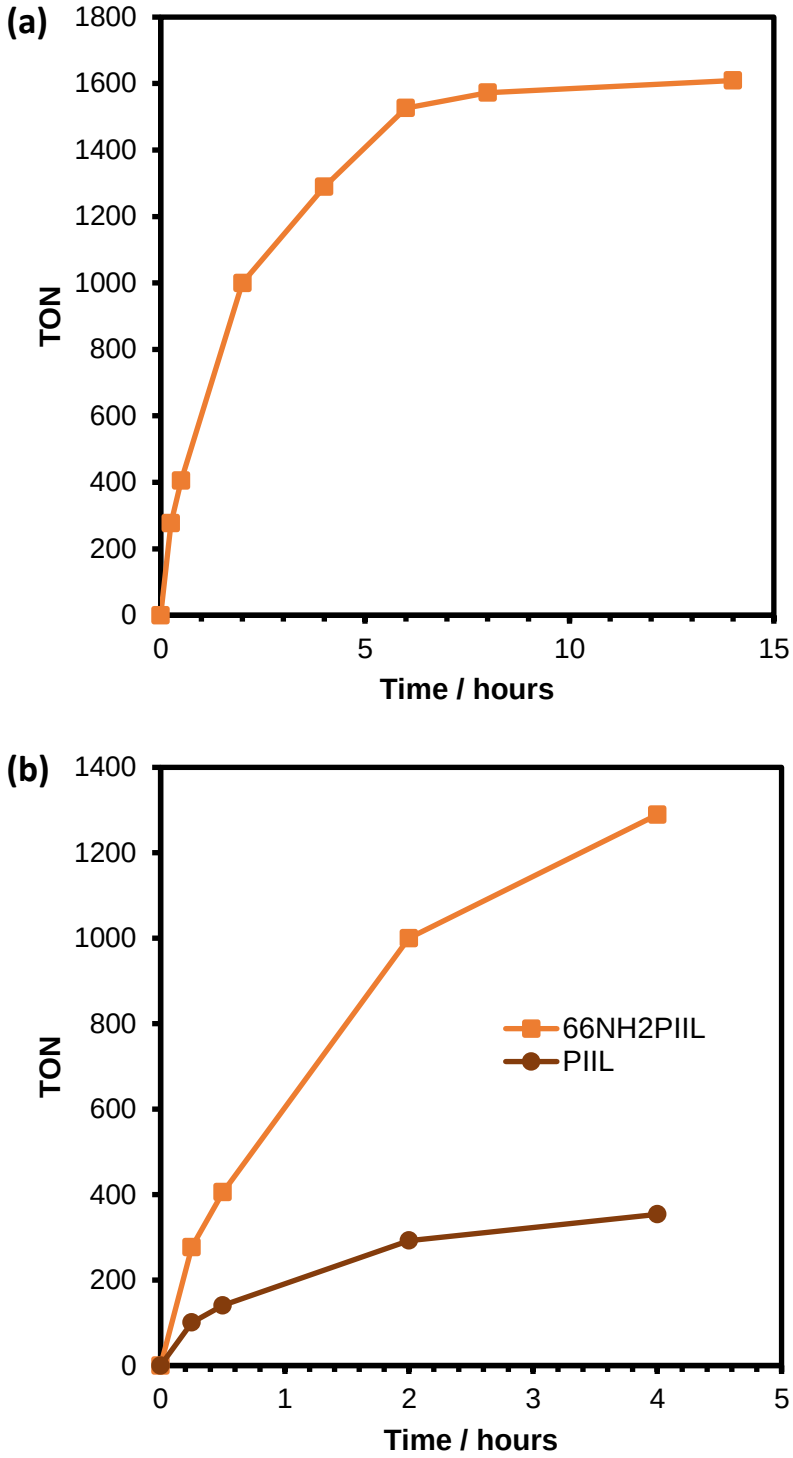

Figure S3 (a) Activity time profile of CO_2 hydrogenation reactions catalysed by **2b.66** (6 µmol Pd), at 100 °C with 40 bar of a 1:1 gas mixture of H_2 : CO_2, in the presence of K_2CO_3 (0.65 M), and the corresponding comparison with **2a** after 4 hours of catalysis (b). Conversion to formate was analysed from batch reactions.

Solution State ^{1}H NMR Spectra of PIIL Supports Recorded in *d4*-MeOH

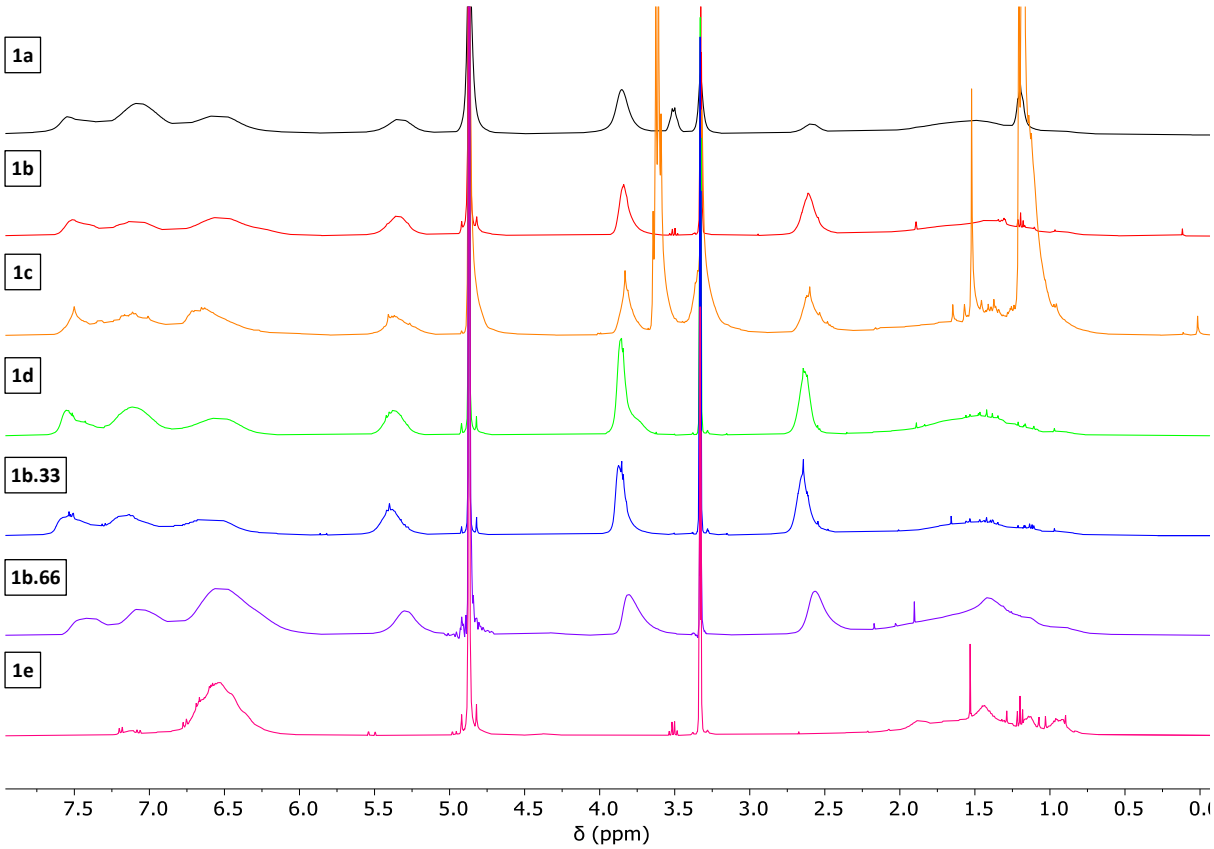

Figure S4 Stacked ^{1}H NMR spectra of polymers **1a-e**

Solid state $^{13}C\{^{1}H\}$ NMR Spectra

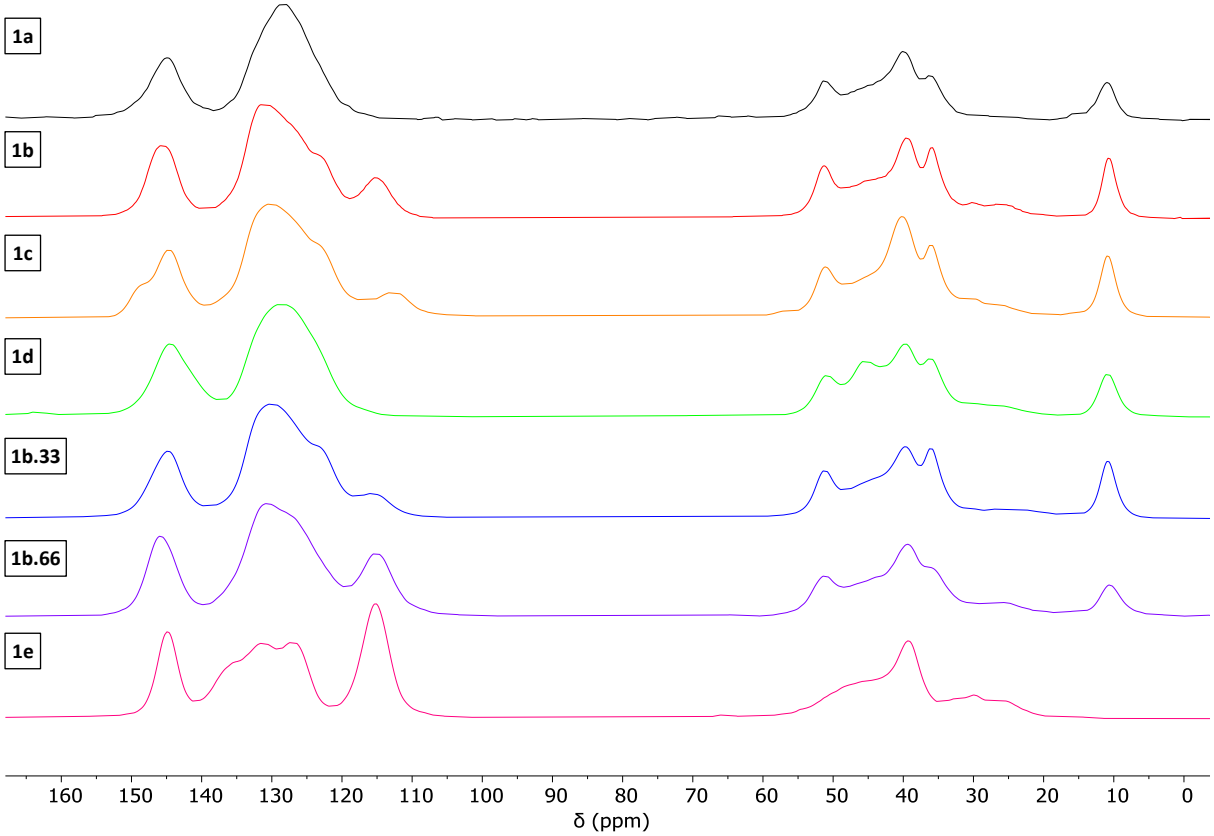

Figure S5 Stacked CP-TOSS MAS ^{13}C NMR spectra of polymers **1a-e**.

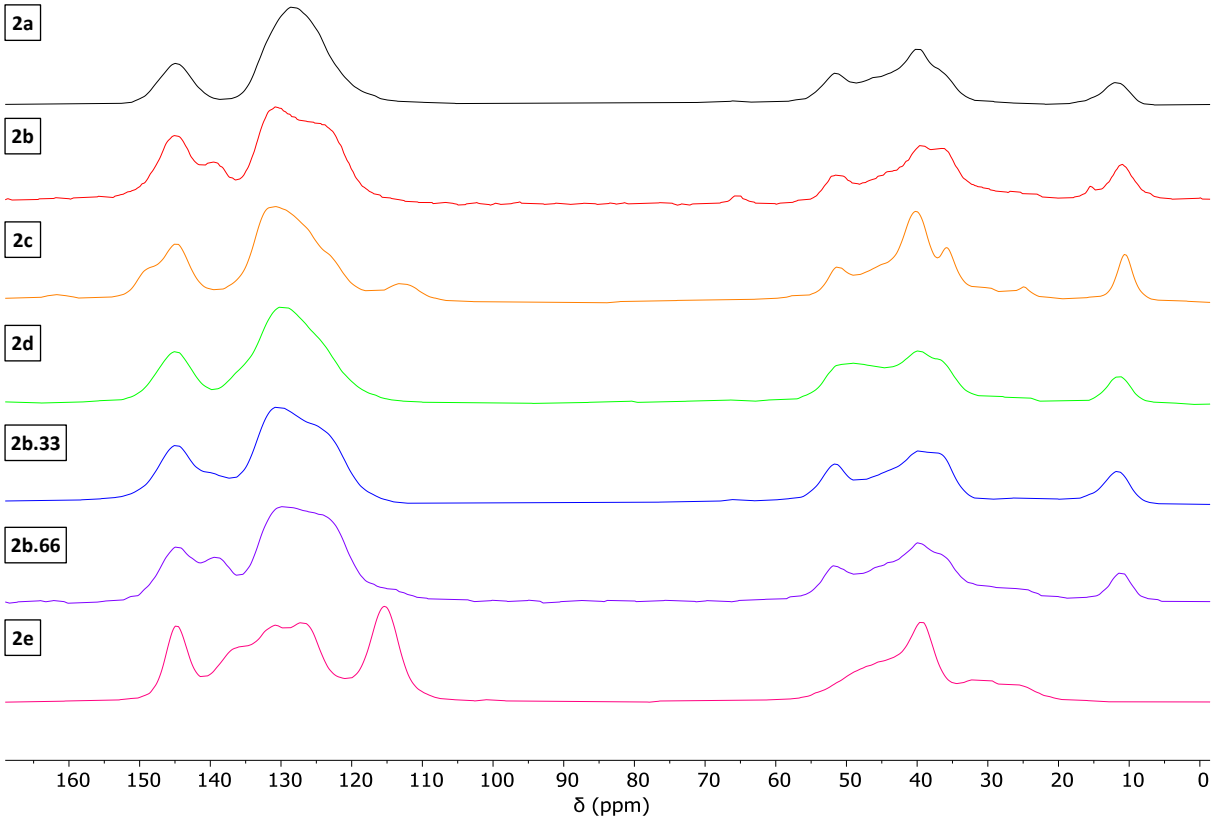

Figure S6 Stacked CP-TOSS MAS ^{13}C NMR spectra of precatalysts **2a-e**.

Solid-State ^{15}N NMR Spectra

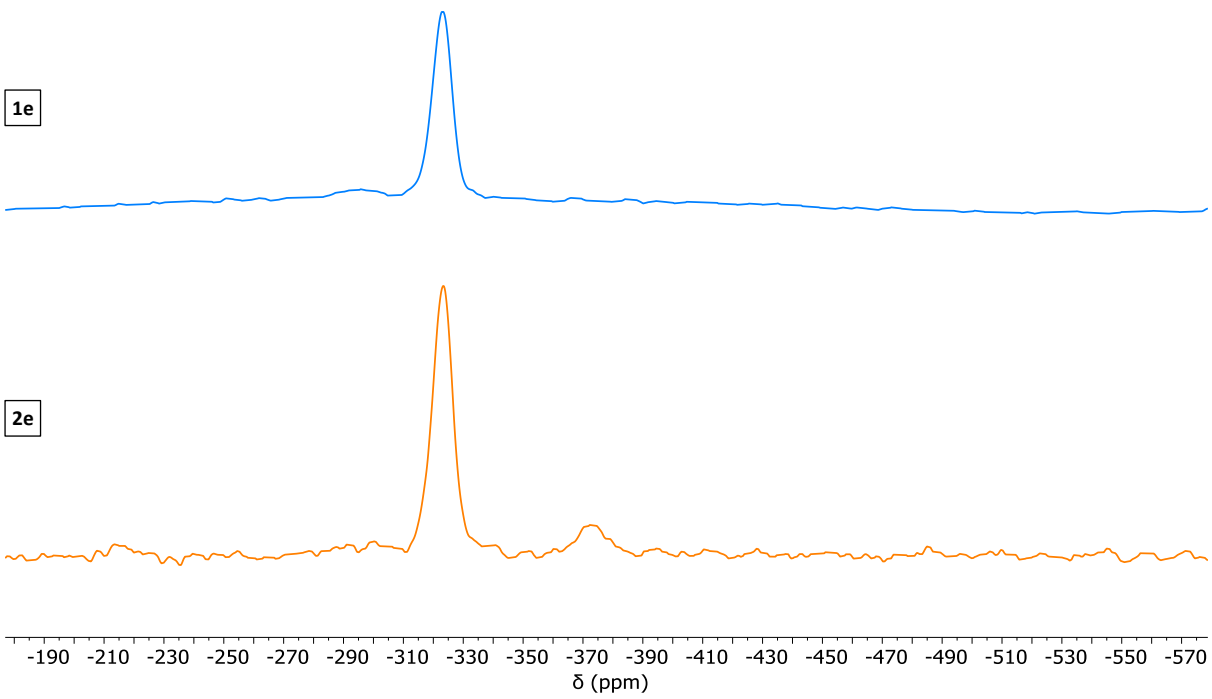

Figure S7 CP-MAS ^{15}N NMR spectra of **1e** (blue) and **2e** (orange).

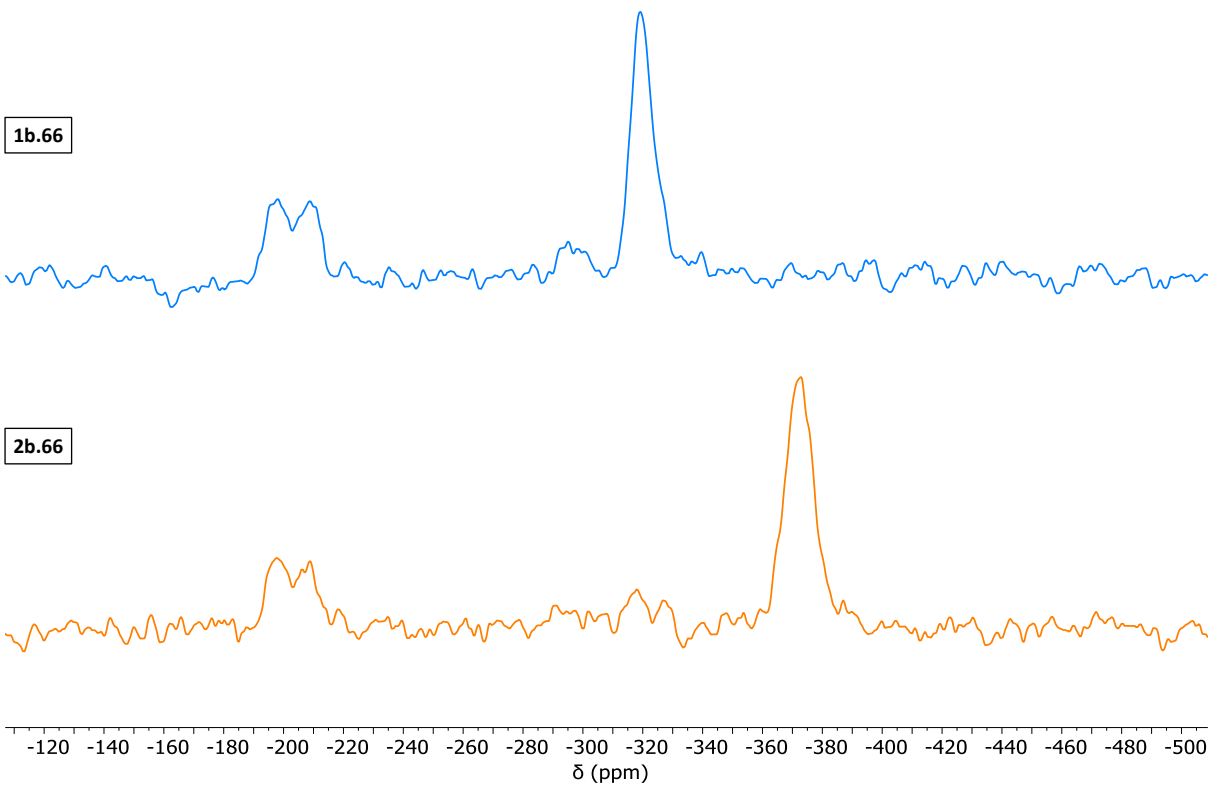

Figure S8 CP-MAS ^{15}N NMR spectra of **1b.66** (blue) and **2b.66** (orange).

FT-IR Spectra

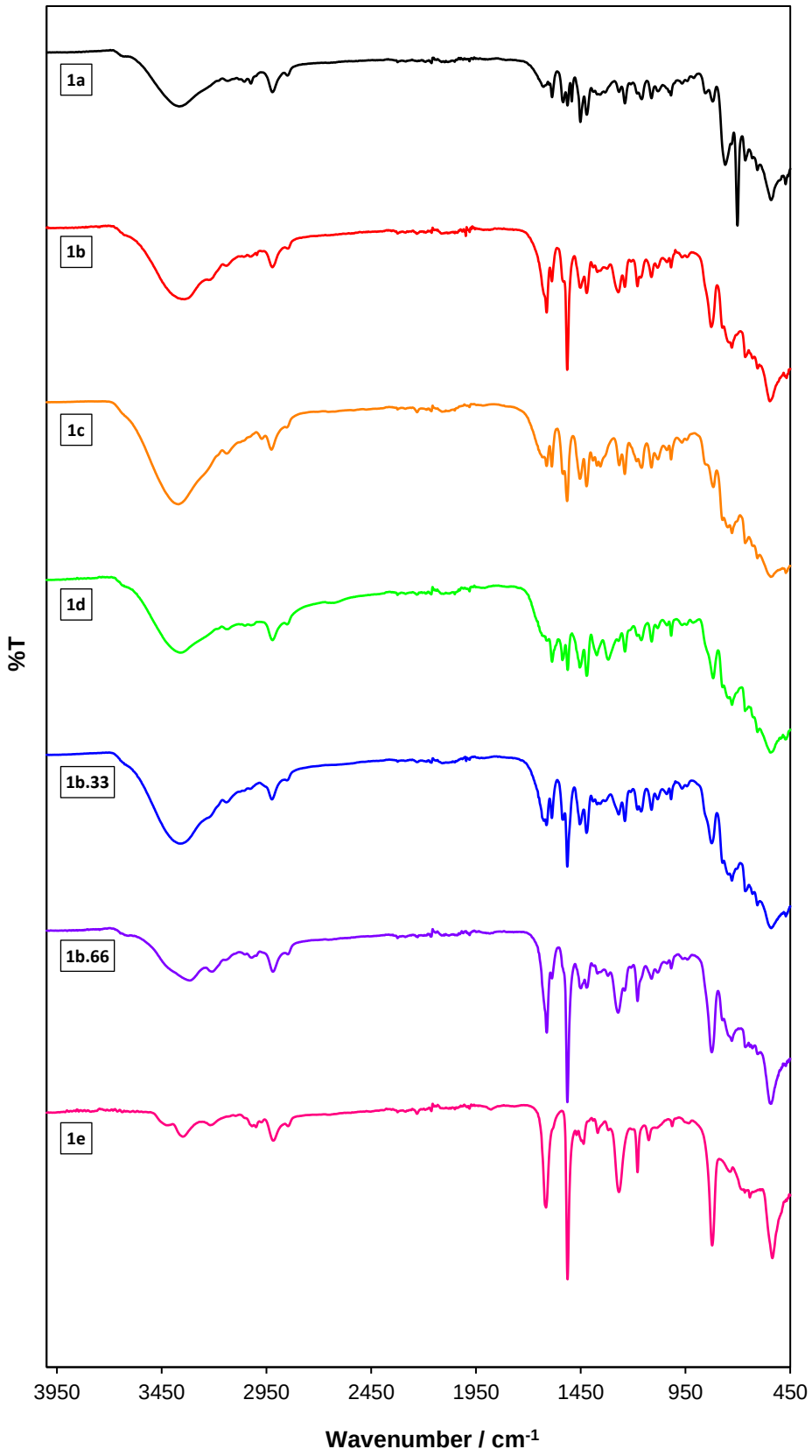

Figure S9 Stacked FT-IR spectra of polymers **1a-e**.

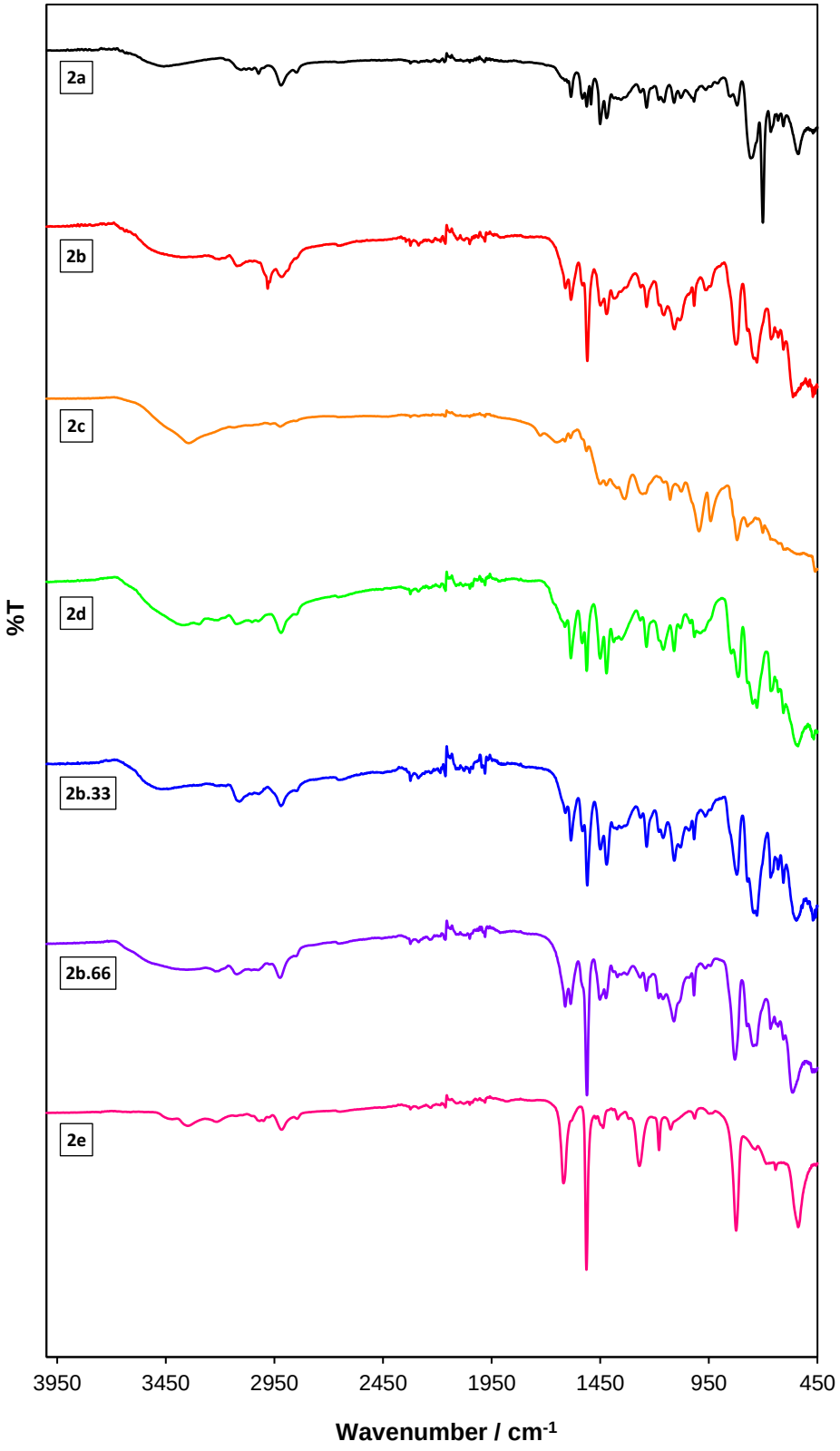

Figure S10 Stacked FT-IR spectra of precatalysts **2a-e**.

SEM Images of Freshly Prepared Polymers and Precatalysts

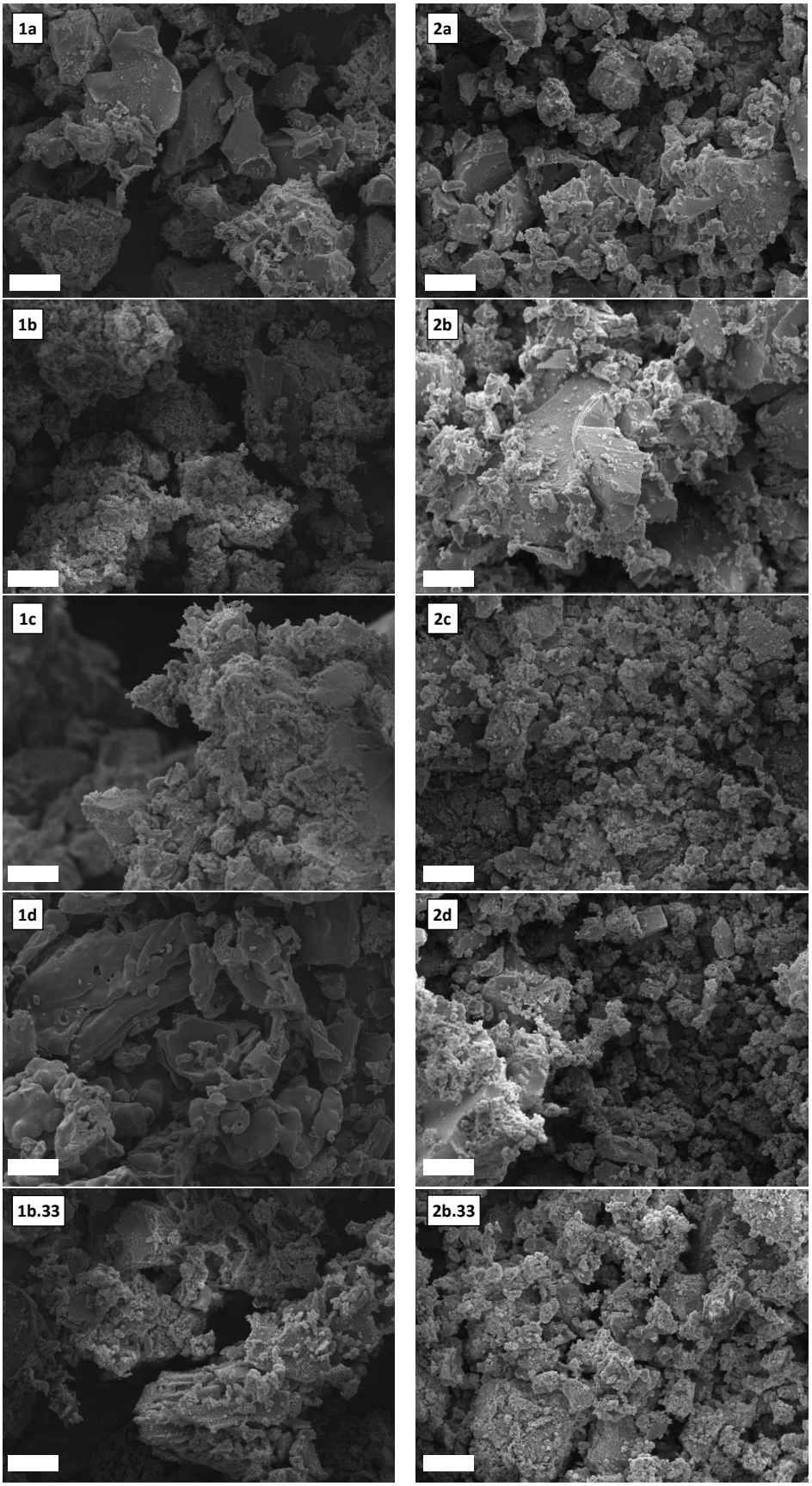

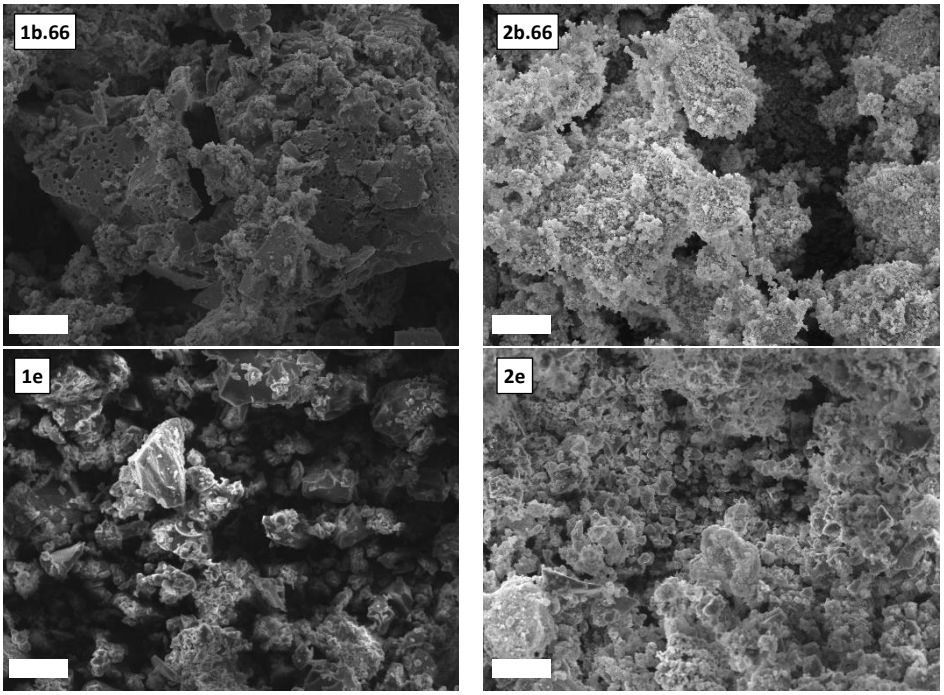

Figure S11 SEM images of polymers **1a-e** and precatalysts **2a-e**; scale bar is 20 μm.

TEM Images of Nanoparticles Generated from Precatalysts 2a-e

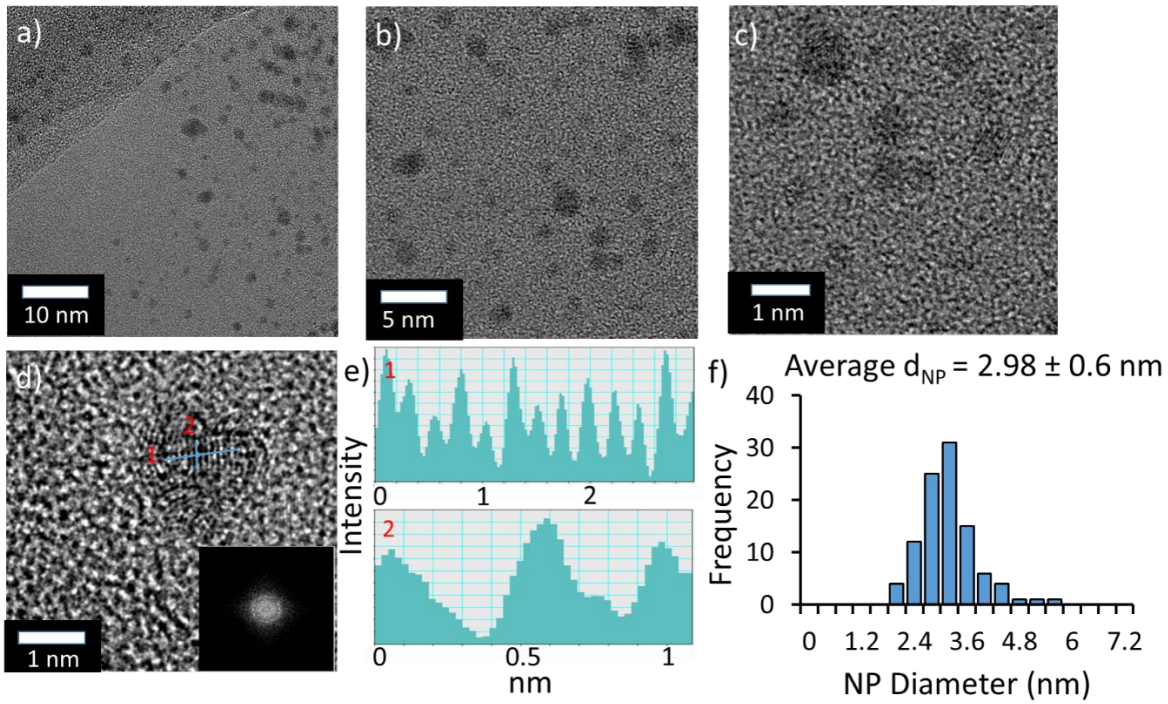

Figure S12 (a-d) High resolution TEM images of PdNPs generated from **2a**, with FFT inset (d), line profiles from the HRTEM image (e) and the corresponding size distribution determined by counting >100 particles. Scale bars are 10-1 nm.

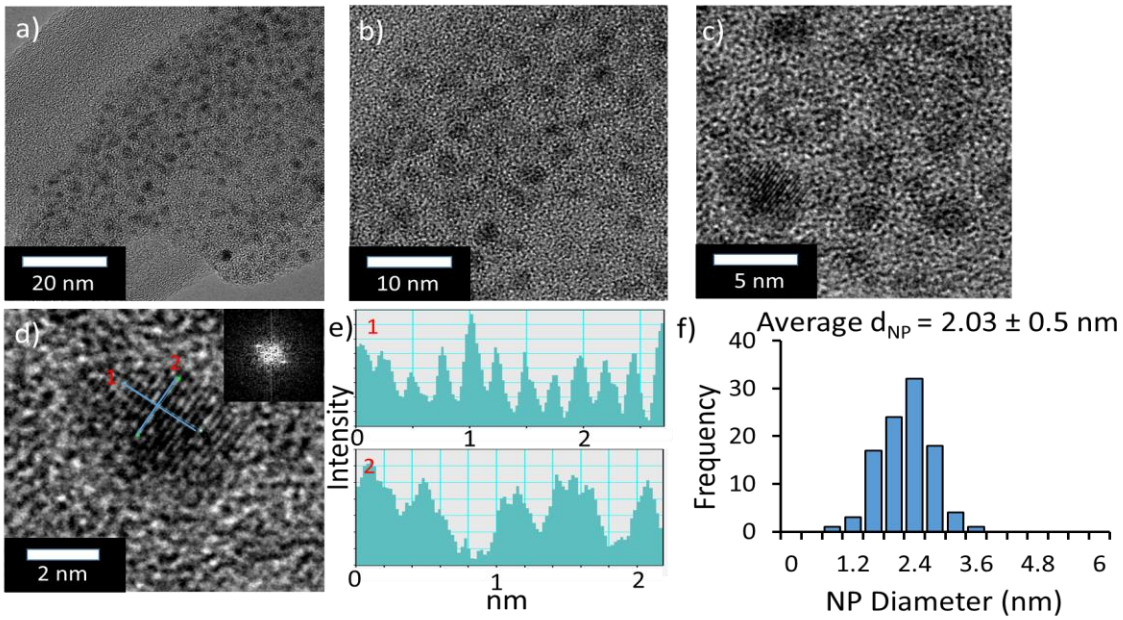

Figure S13 (a-d) High resolution TEM images of PdNPs generated from **2b**, with FFT inset (d), line profiles from the HRTEM image (e) and the corresponding size distribution determined by counting >100 particles. Scale bars are 20-2 nm.

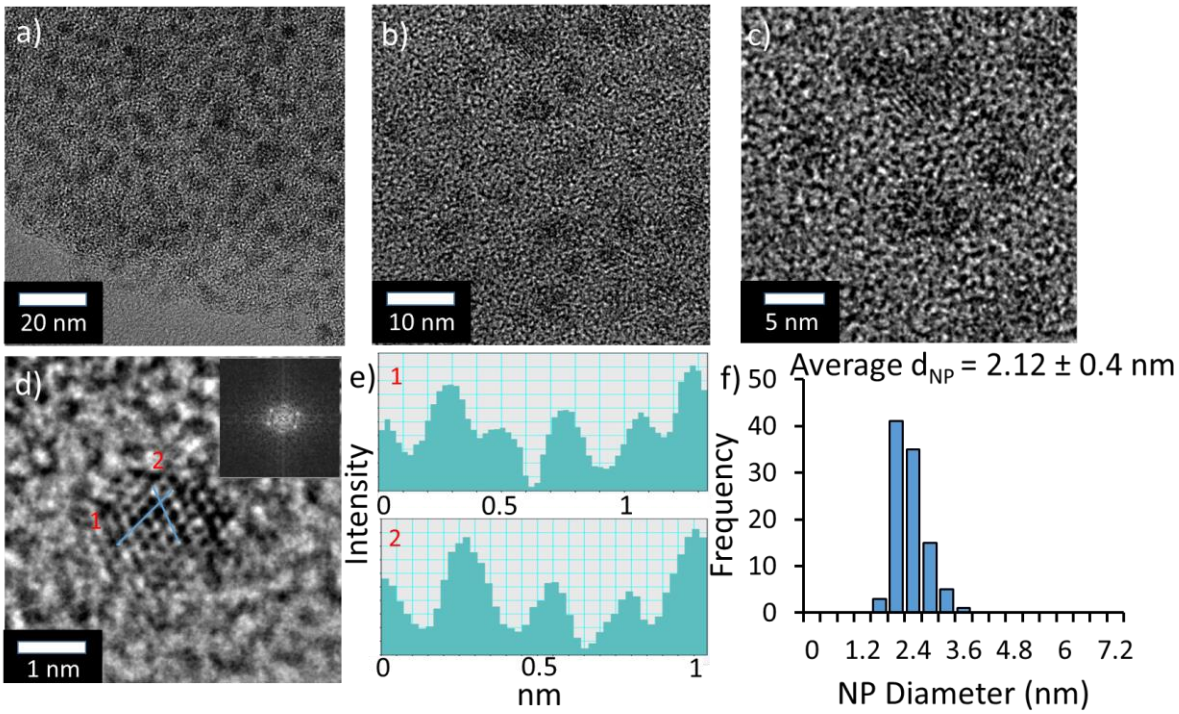

Figure S14 (a-d) High resolution TEM images of PdNPs generated from **2b.33**, with FFT inset (d), line profiles from the HRTEM image (e) and the corresponding size distribution determined by counting >100 particles. Scale bars are 20-1 nm.

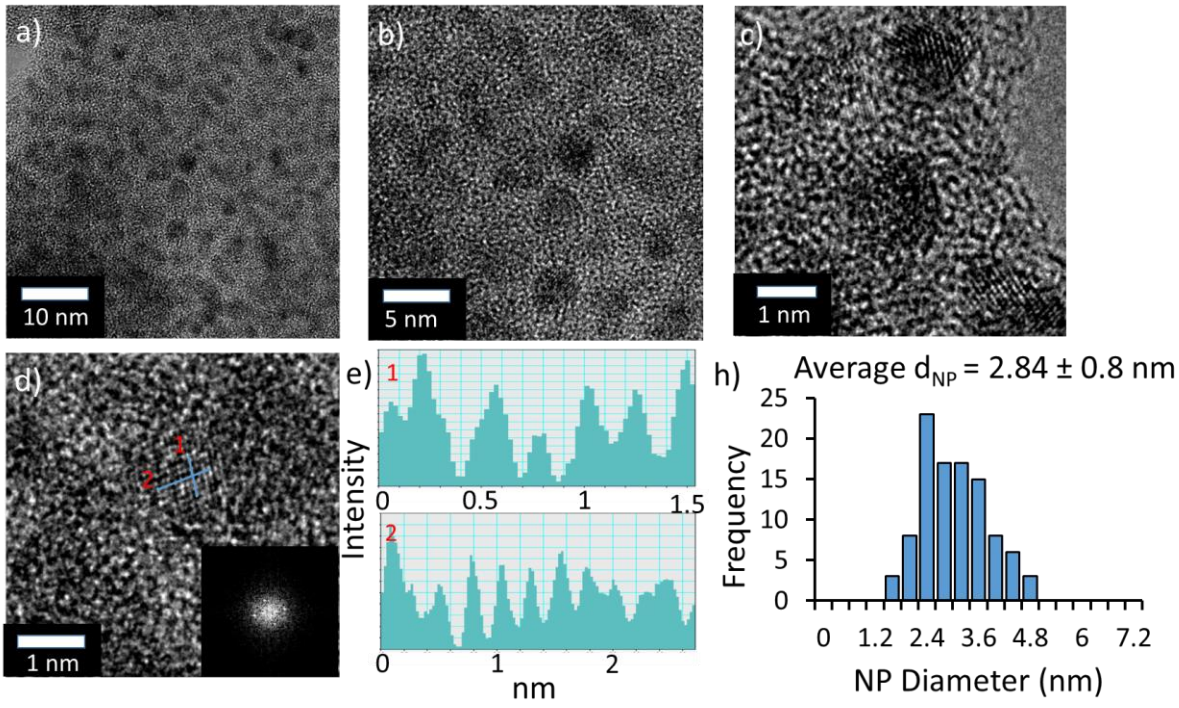

Figure S15 (a-d) High resolution TEM images of PdNPs generated from **2b.66**, with FFT inset (d), line profiles from the HRTEM image (e) and the corresponding size distribution determined by counting >100 particles. Scale bars are 10-1 nm.

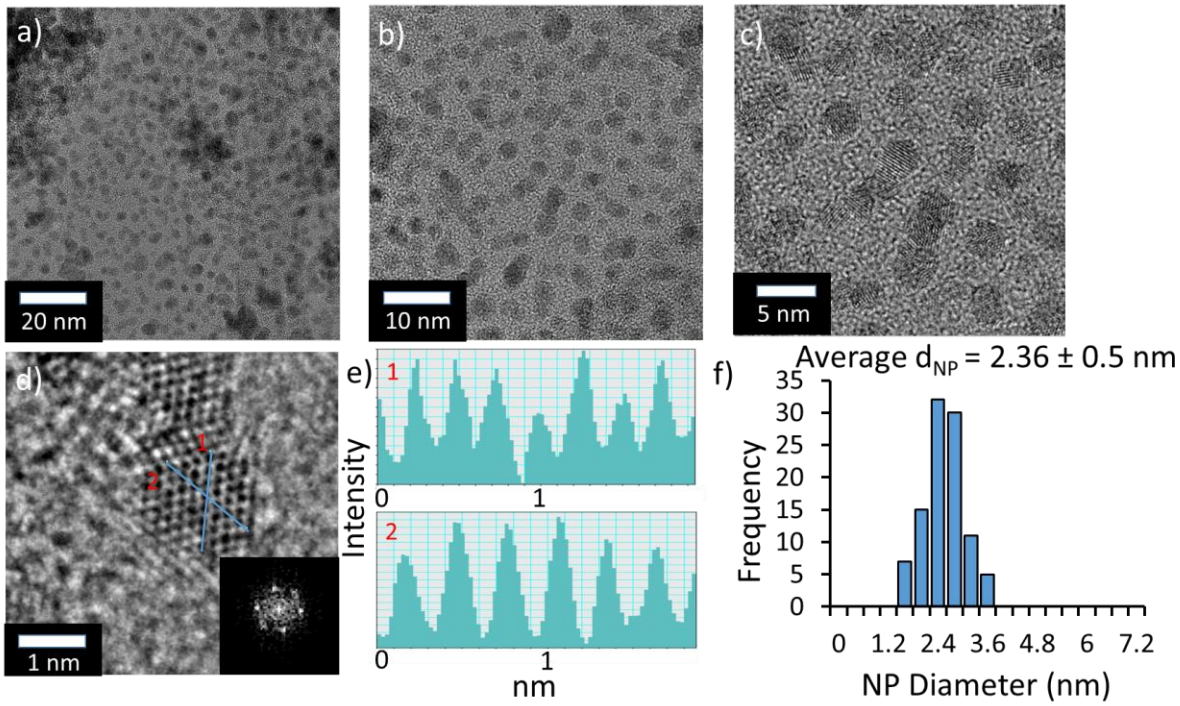

Figure S16 (a-d) High resolution TEM images of PdNPs generated from **2c**, with FFT inset (d), line profiles from the HRTEM image (e) and the corresponding size distribution determined by counting >100 particles. Scale bars are 20-1 nm.

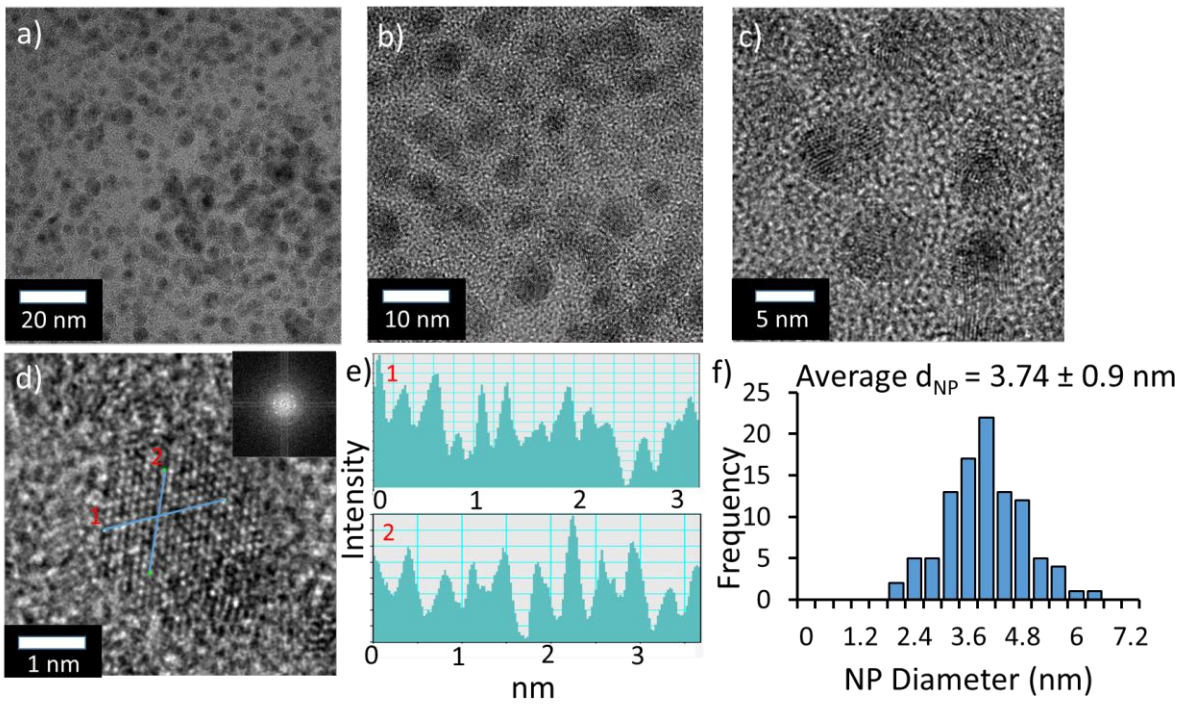

Figure S17 (a-d) High resolution TEM images of PdNPs generated from **2d**, with FFT inset (d), line profiles from the HRTEM image (e) and the corresponding size distribution determined by counting >100 particles. Scale bars are 20-1 nm.

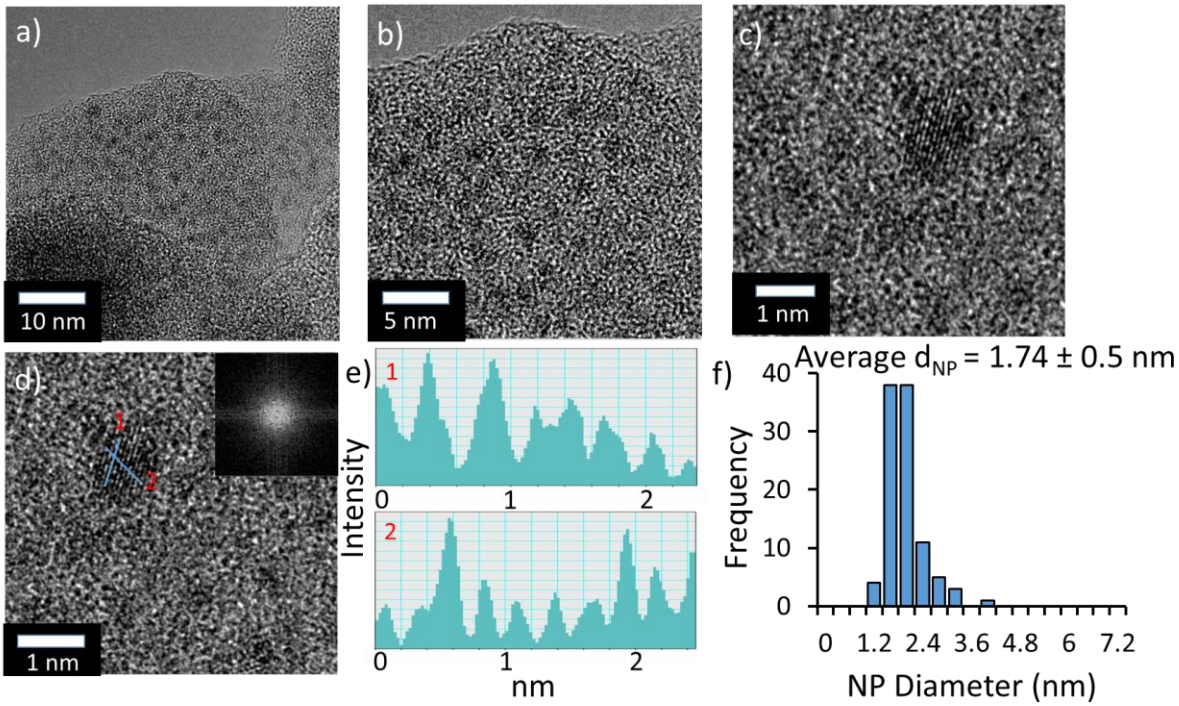

Figure S18 (a-d) High resolution TEM images of PdNPs generated from **2e**, with FFT inset (d), line profiles from the HRTEM image (e) and the corresponding size distribution determined by counting >100 particles. Scale bars are 10-1 nm.

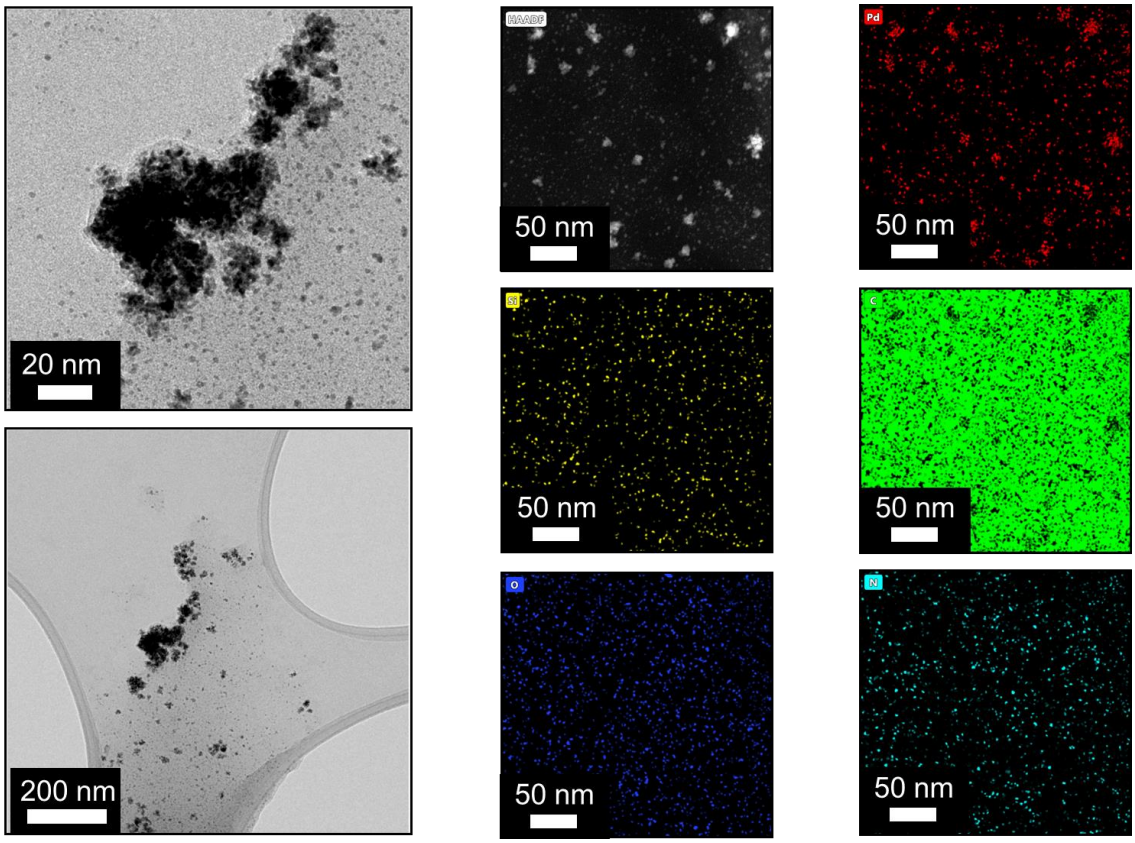

Figure S19 (left) Large field of view TEM images of PdNPs generated from **2a**. (right) HAADF-STEM image and individual EDX maps of **2a** showing Pd (red), Si (yellow), C (green), O (blue) and N (turquoise).

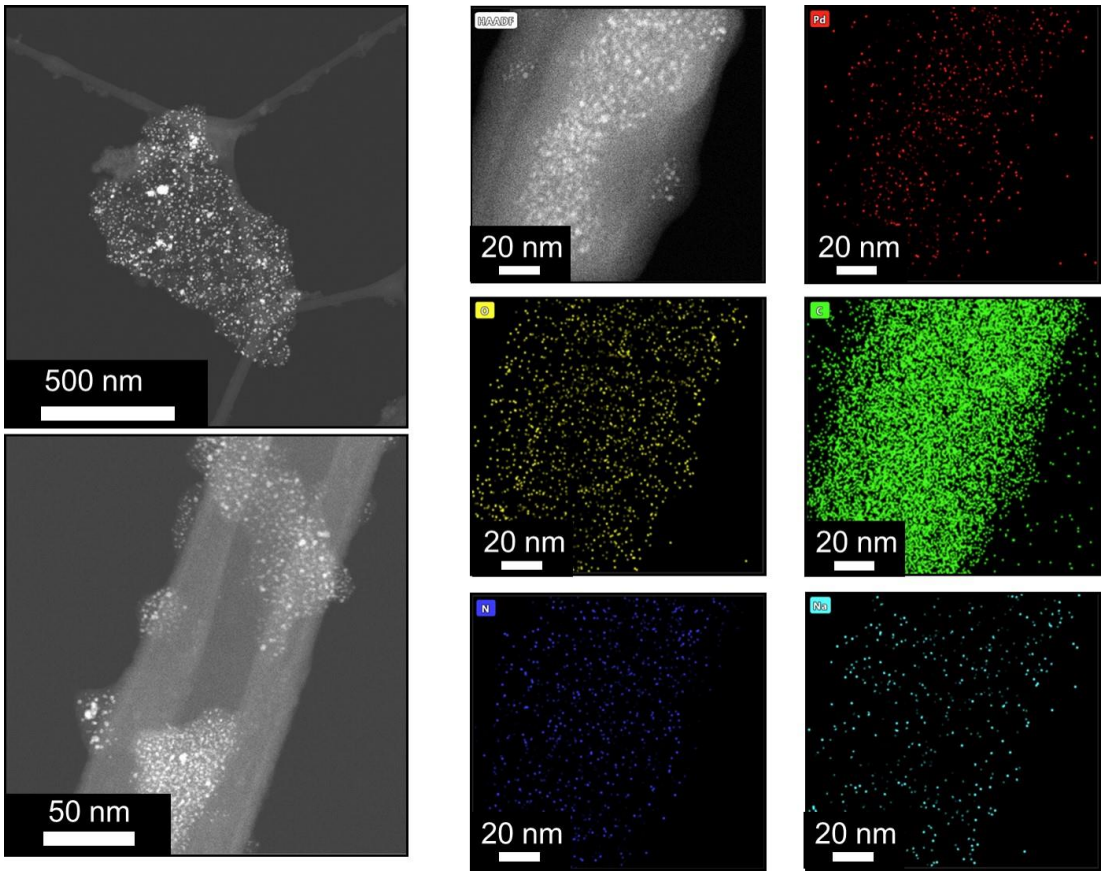

Figure S20 (left) Large field of view TEM images of PdNPs generated from **2b**. (right) HAADF-STEM image and individual EDX maps of **2b** showing Pd (red), Si (yellow), C (green), O (blue) and N (turquoise).

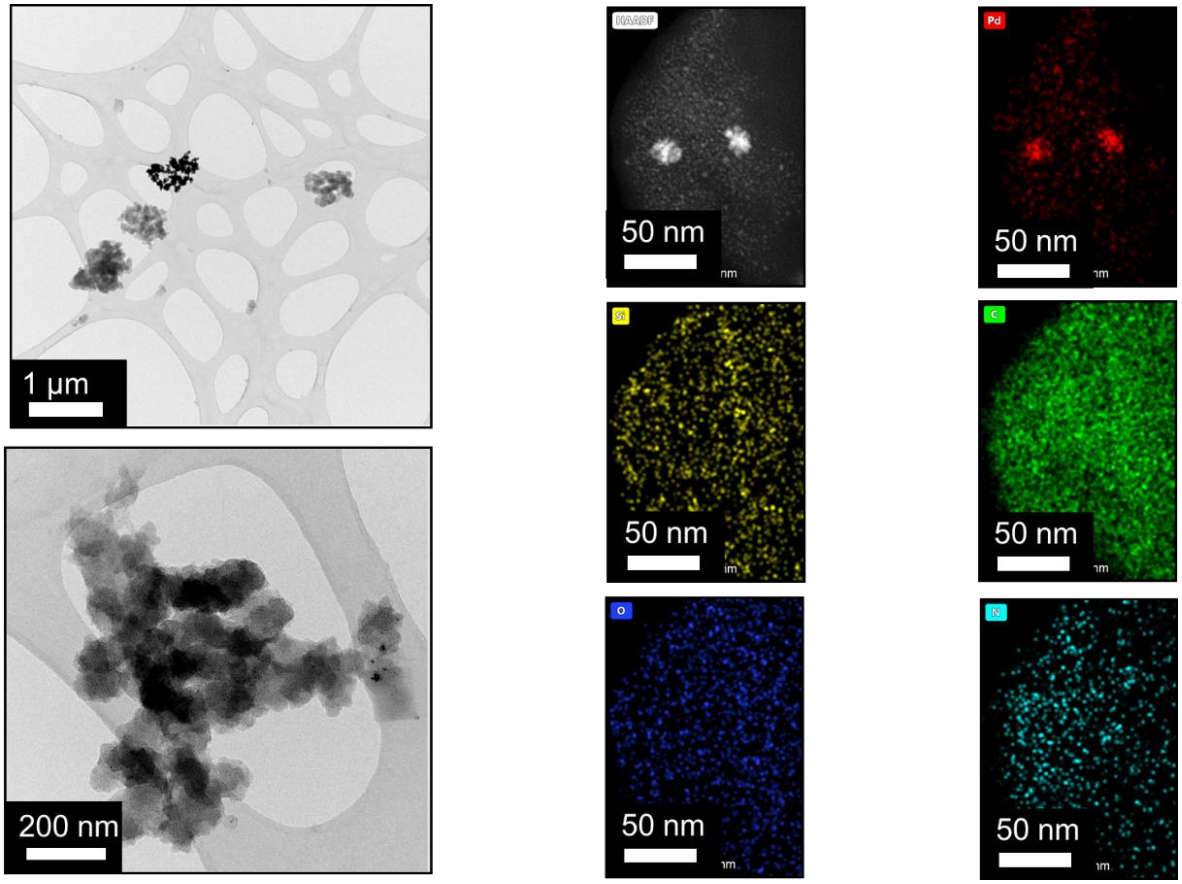

Figure S21 (left) Large field of view TEM images of PdNPs generated from **2b.33**. (right) HAADF-STEM image and individual EDX maps of **2b.33** showing Pd (red), Si (yellow), C (green), O (blue) and N (turquoise).

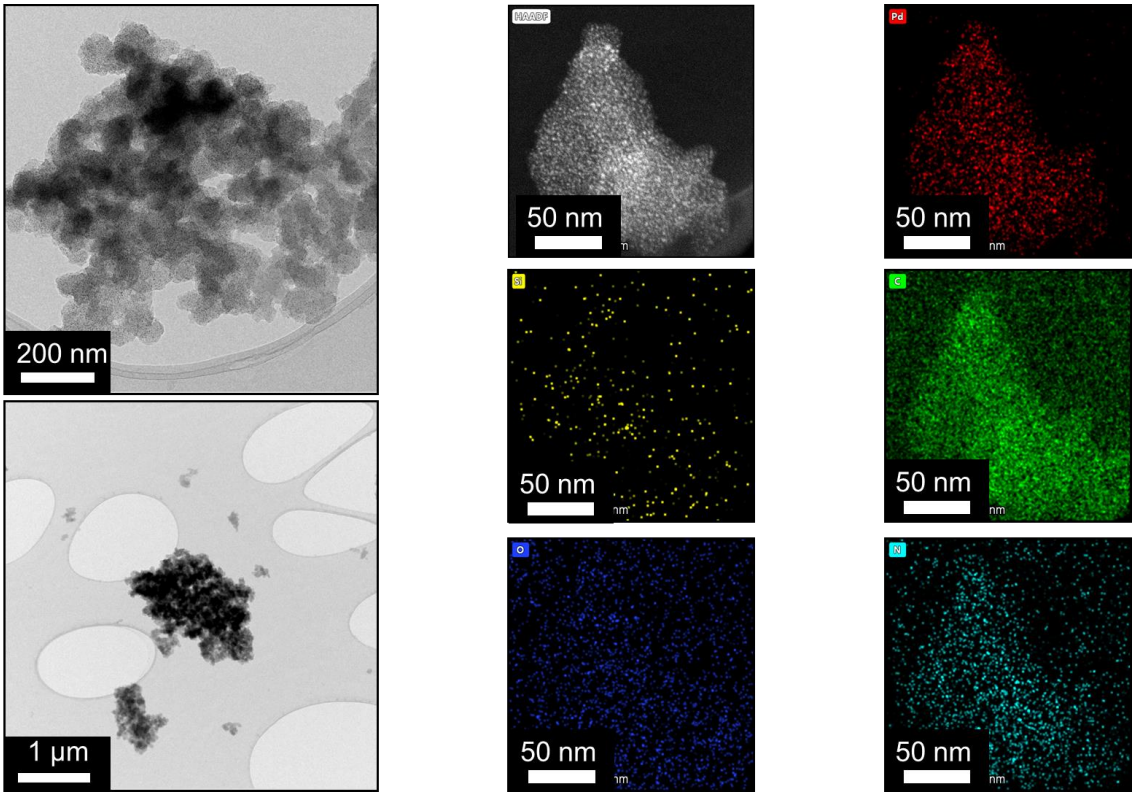

Figure S22 (left) Large field of view TEM images of PdNPs generated from **2b.66**. (right) HAADF-STEM image and individual EDX maps of **2b.66** showing Pd (red), Si (yellow), C (green), O (blue) and N (turquoise).

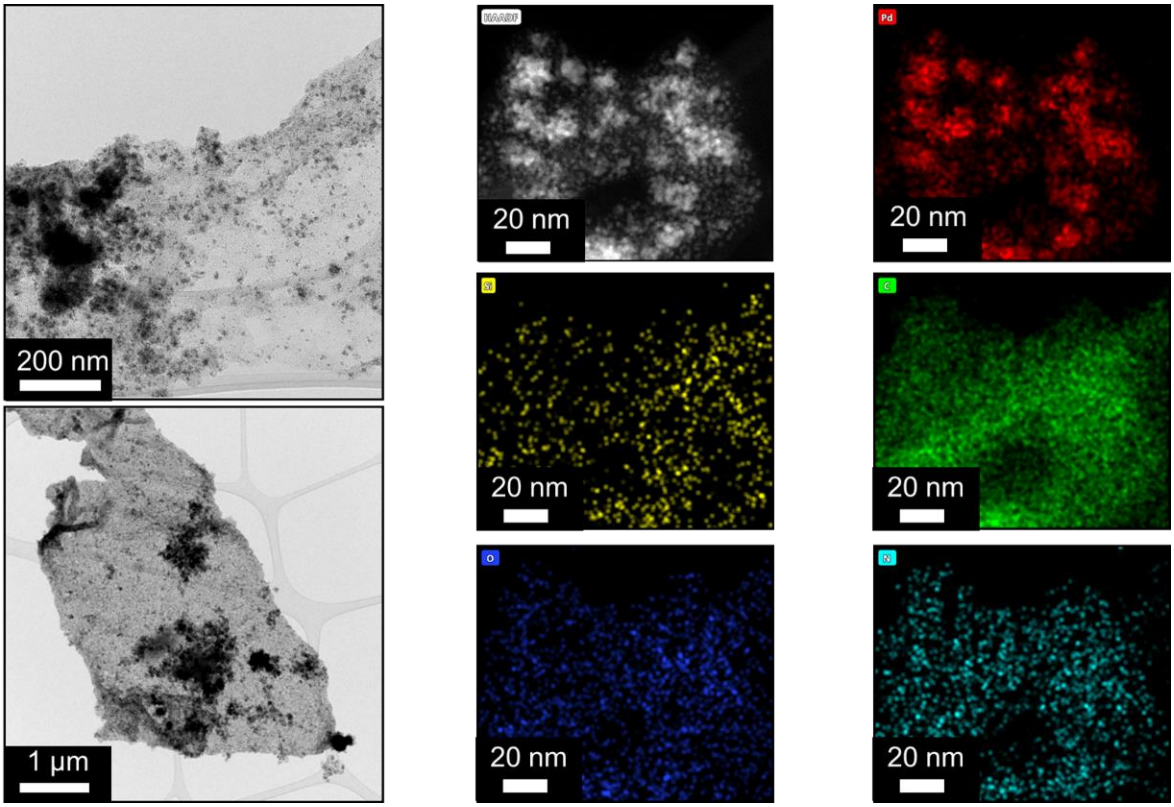

Figure S23 (left) Large field of view TEM images of PdNPs generated from **2c**. (right) HAADF-STEM image and individual EDX maps of **2c** showing Pd (red), Si (yellow), C (green), O (blue) and N (turquoise).

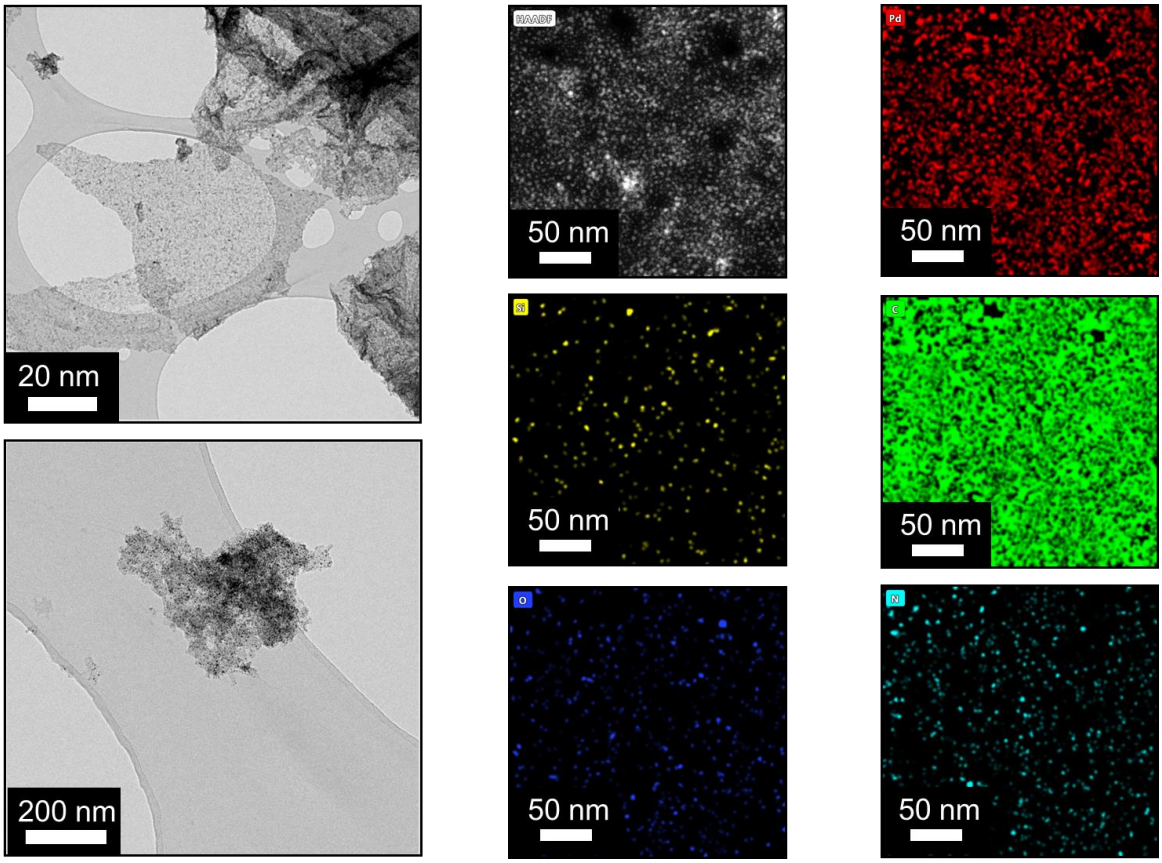

Figure S24 (left) Large field of view TEM images of PdNPs generated from **2d**. (right) HAADF-STEM image and individual EDX maps of **2d** showing Pd (red), Si (yellow), C (green), O (blue) and N (turquoise).

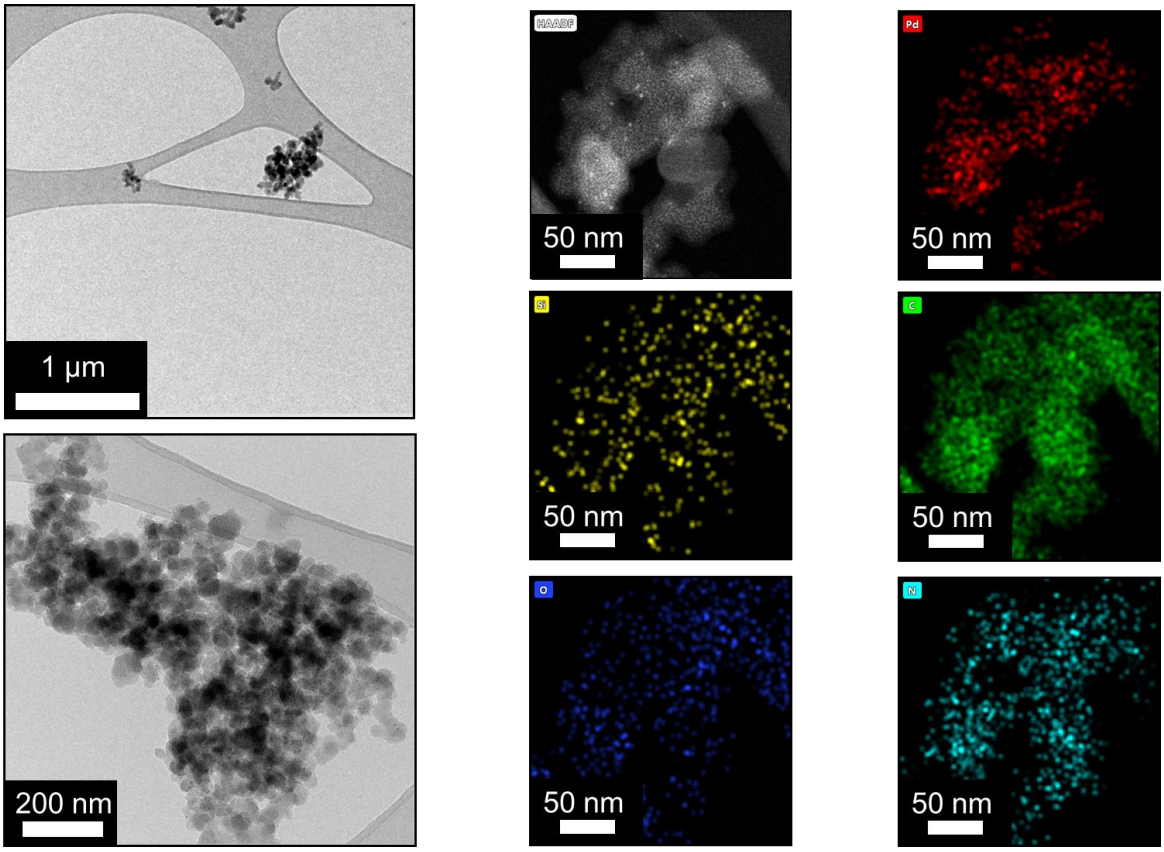

Figure S25 (left) Large field of view TEM images of PdNPs generated from **2e**. (right) HAADF-STEM image and individual EDX maps of **2e** showing Pd (red), Si (yellow), C (green), O (blue) and N (turquoise).

XPS Characterisation

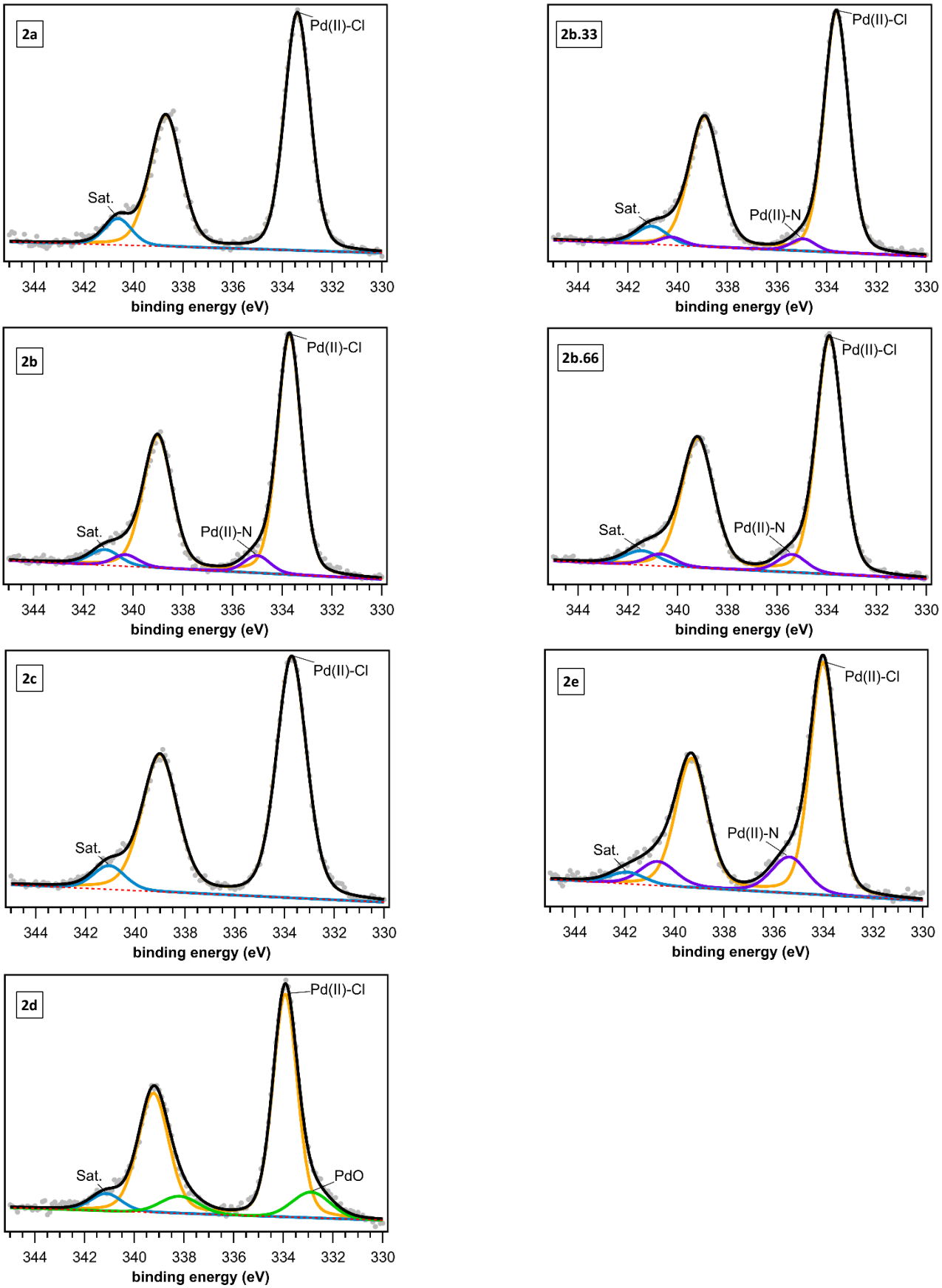

Figure S26 Pd 3d core level XPS spectra of precatalysts **2a-e**.

Table S2 Pd 3d binding energies with relative abundance of each species for precatalysts **2a-e**, where Sat. = shake-up satellite.

Sample	Pd(II)-Cl	Sat.	Pd(II)-N	PdO	Pd(II)-Cl	Sat.	Pd(II)-N	PdO
	$3d_{5/2}$		$3d_{5/2}$	$3d_{5/2}$	%	%	%	%
2a	333.4	340.6			93	7		
2b	333.7	340.1	335.0		89	4	7	
2c	333.7	341.1			94	6		
2d	333.9	341.1		332.9	82	5		13
2b.33	333.6	341.0	335.0		91	5	4	
2b.66	333.9	341.4	335.4		88	4	7	
2e	334.0	341.9	335.4		80	3	17	

For sample **2d**, the P1 (divalent $PdCl_4$) and P4 signals show a separation of 1.05 eV which is consistent with previous reports of Pd(II) coordinated with Cl^- in the presence of PdO (0.9 eV).[4]

Table S3 Comparison of binding energy separations between $Pd3d_{5/2}$ (P1 from Table SX) and N1s imidazolium, as well as between Pd(II)-Cl ($3d_{5/2}$) and C1s (aliphatic) for precatalysts **2a-d**.

Precatalyst	Support	ΔPd-N / eV	ΔPd-C / eV
2a	PIIL	64.0	52.8
2b	NH_2PIIL	63.8	53.1
2c	NMe_2PIIL	63.9	53.0
2d	NH_2CH_2PIIL	63.6	53.3

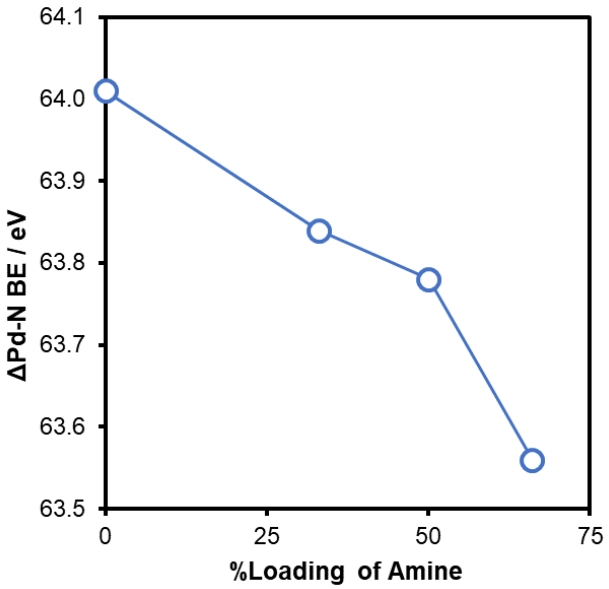

Figure S27 Plot of binding energy difference between the Pd(II)-Cl ($3d_{5/2}$) and the imidazolium N 1s core electrons against the mol% loading of amine on the precatalyst support for precatalysts **2a**, **2b.33**, **2b.66**.

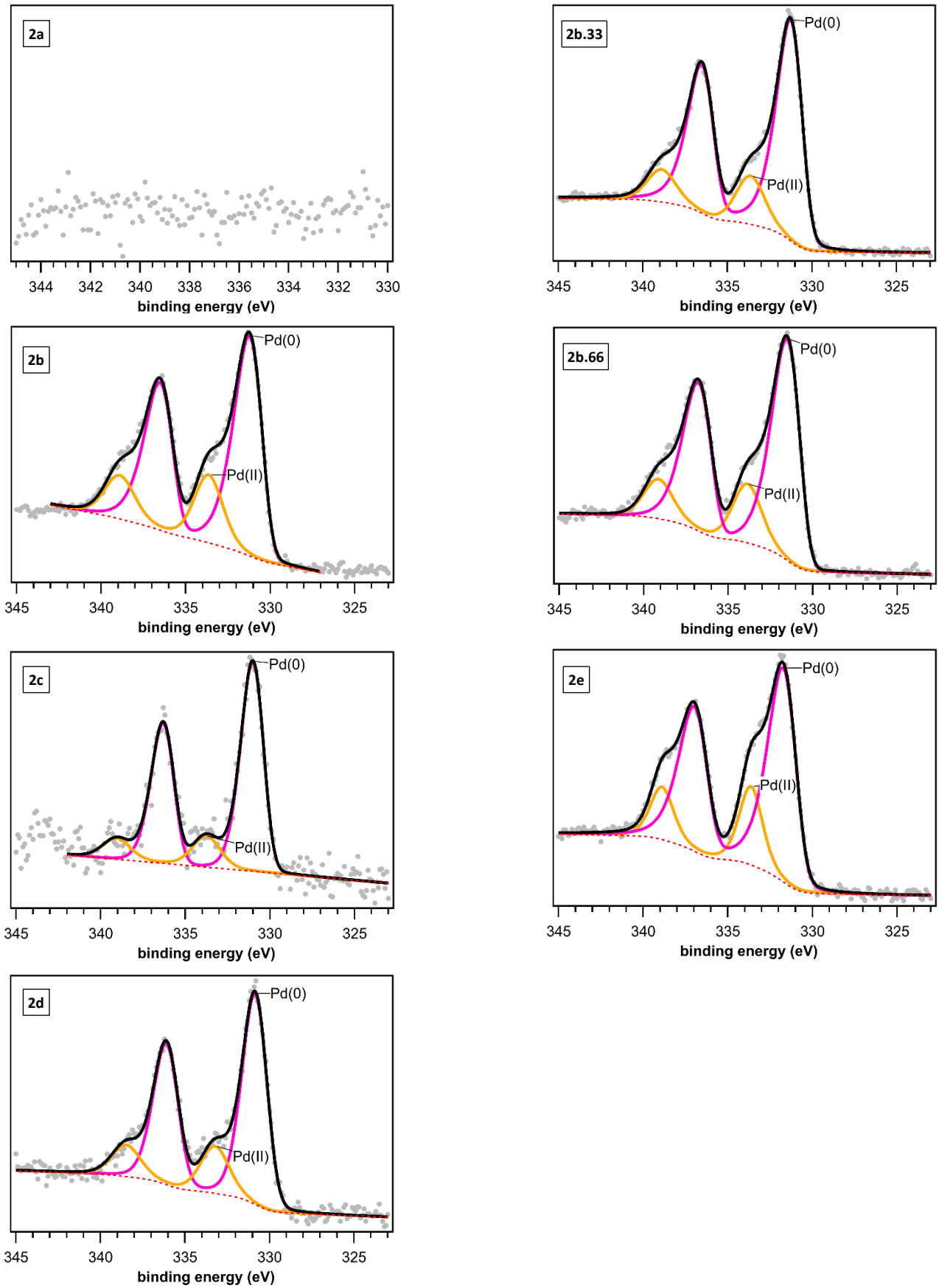

Figure S28 Pd 3d core level XPS spectra of catalysts generated from precatalysts **2a-e** after 2 hours of hydrogenation.

Table S4 Pd 3d binding energies with relative abundance of each component for catalysts generated from precatalysts **2a-e** after 2 hours of hydrogenation.

Sample	Pd(II)-Cl $3d_{5/2}$	Pd(0) $3d_{5/2}$	Pd(II)-Cl %	Pd(0) %
2a NP	-	-	-	-
2b NP	333.6	331.3	22	78
2c NP	333.8	331.1	16	84
2d NP	333.2	330.9	21	79
2b.33 NP	333.6	331.4	20	80
2b.66 NP	333.9	331.6	22	78
2e NP	333.6	331.8	24	76

Fitting of **2c NP** restricted to a maximum of 342 eV due to the presence of an apparent calcium contaminant at 343.5 eV.

Table S5 Binding energy separations between Pd(II) coordinated to Cl ($3d_{5/2}$) and C1s (aliphatic), as well as between Pd(0) and C 1s (aliphatic).

Catalyst	**Support**	**ΔPd(II)-C /eV**	**ΔPd(0)-C /eV**
2a NP	PIIL	-	-
2b NP	NH_2PIIL	53.1	50.8
2c NP	NMe_2PIIL	53.1	50.4
2d NP	NH_2CH_2PIIL	52.6	50.2

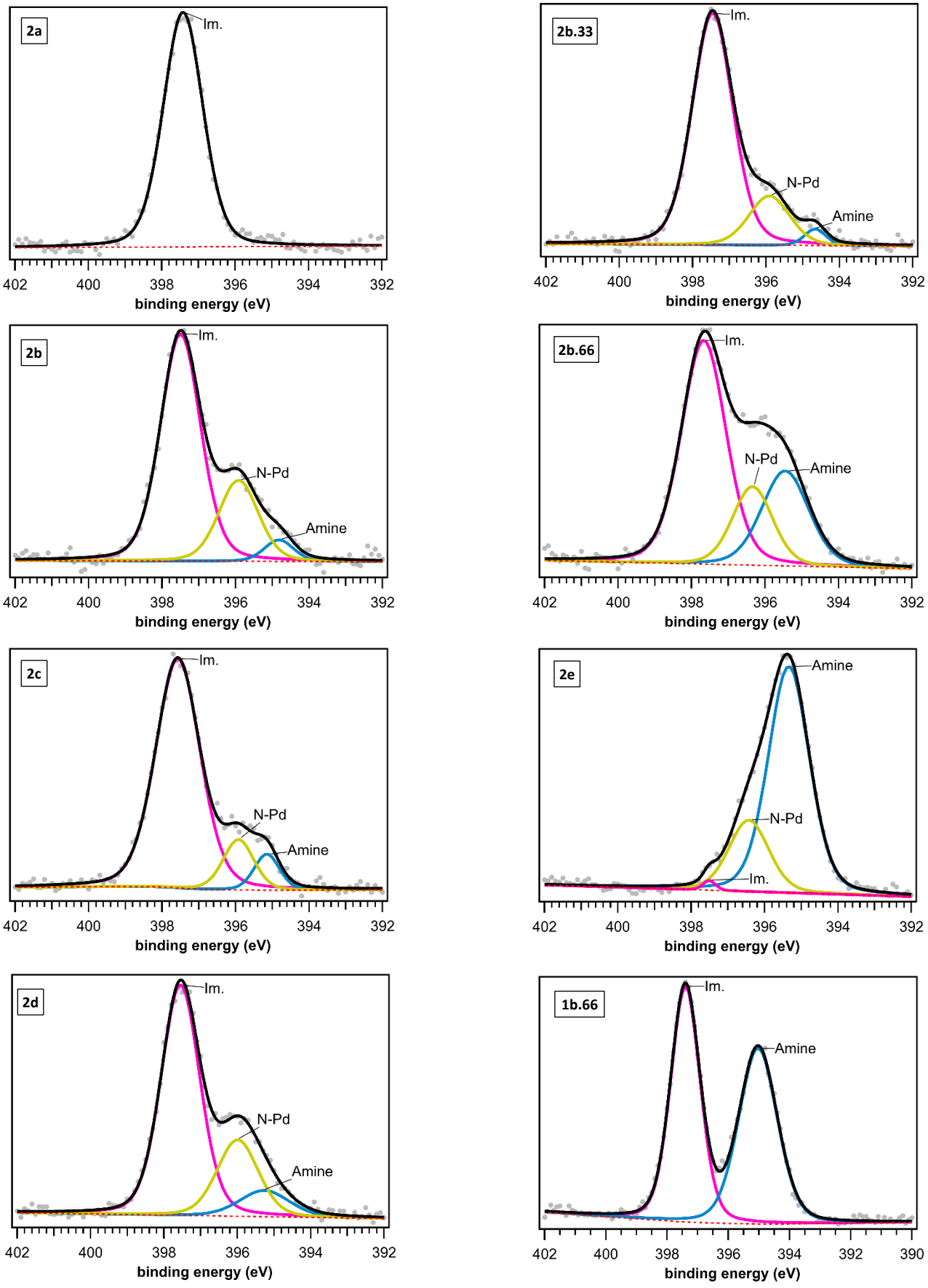

Figure S29 N 1s core level XPS spectra of precatalysts **2a-e** and polymer **1b.66**.

Table S6 N 1s binding energies with relative abundance of each species for precatalysts **2a-e.**

Sample	Imidazolium	Amine	N-Pd	Imidazolium	Amine	N-Pd
				%	%	%
2a	397.4			100		
2b	397.5	394.8	395.9	70	5	25
2c	397.6	395.1	395.9	81	8	12
2d	397.6	395.3	396.0	67	10	23
2b.33	397.5	394.7	395.9	80	3	17
2b.66	397.5	395.5	396.3	57	25	18
2e	397.5	395.3	396.4	1	76	23
1b.66	397.4	395.0		51	49	

The N1s spectrum of sample **2e** shows a small impurity with a binding energy consistent with that of imidazolium (397.5 eV) – as this impurity was in such low abundance (1%), it has been attributed to cross-contamination across samples during analysis.

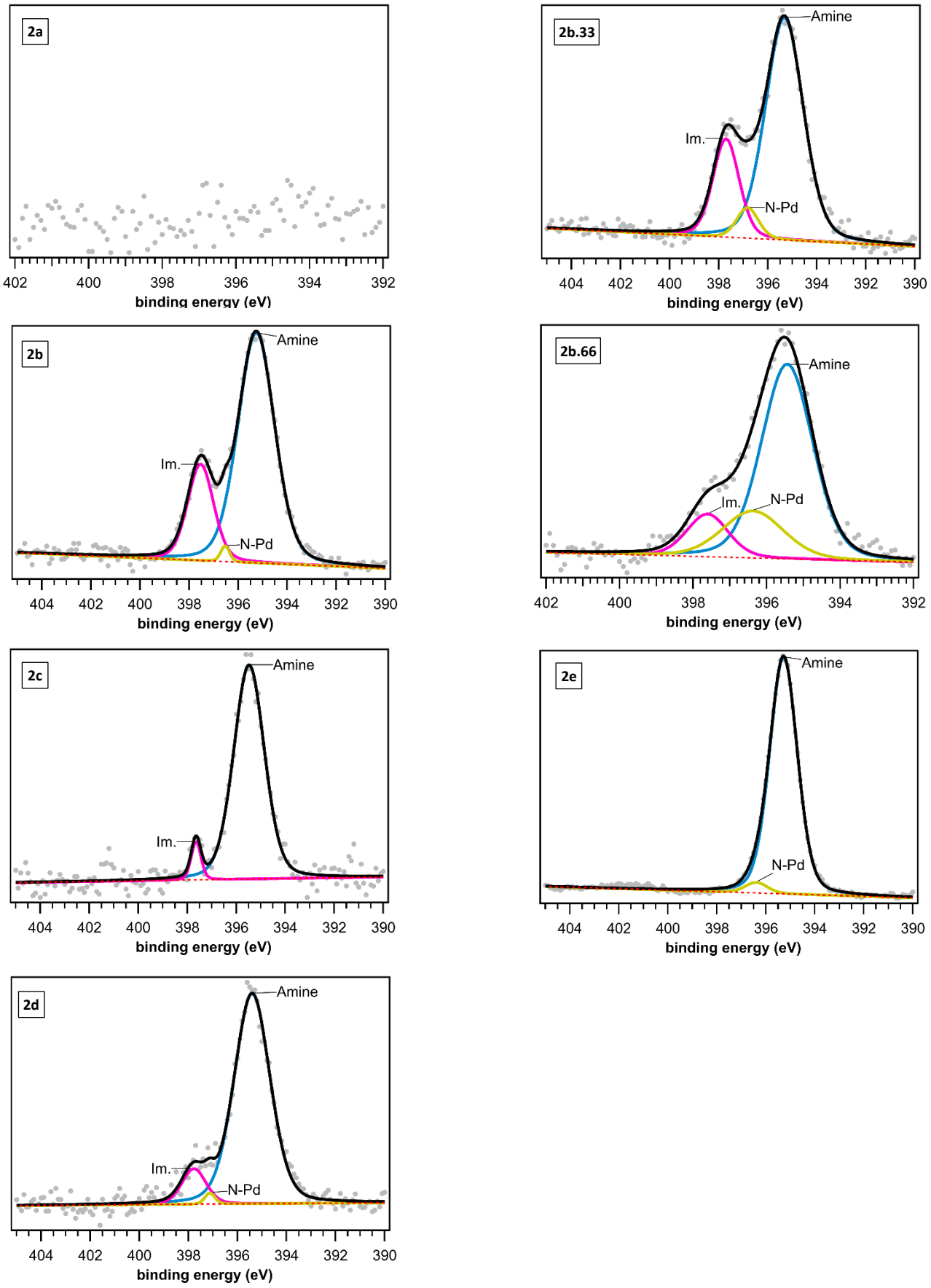

Figure S30 N 1s core level XPS spectra of catalysts generated from precatalysts **2a-e** after 2 hours of hydrogenation.

Table S7 N 1s binding energies with relative abundance of each component for catalysts generated from precatalysts **2a-e** after 2 hours of hydrogenation**.**

Sample	Imidazolium	Amine	N-Pd	Imidazolium	Amine	N-Pd
				%	%	%
2a	-	-	-	-	-	-
2b	397.5	395.3	396.5	23	76	1
2c	397.6	395.5		5	95	
2d	397.8	395.4	397.1	10	89	1
2b.33	397.7	395.3	396.8	22	76	3
2b.66	397.6	395.4	396.4	12	68	20
2e		395.3	395.4		97	3

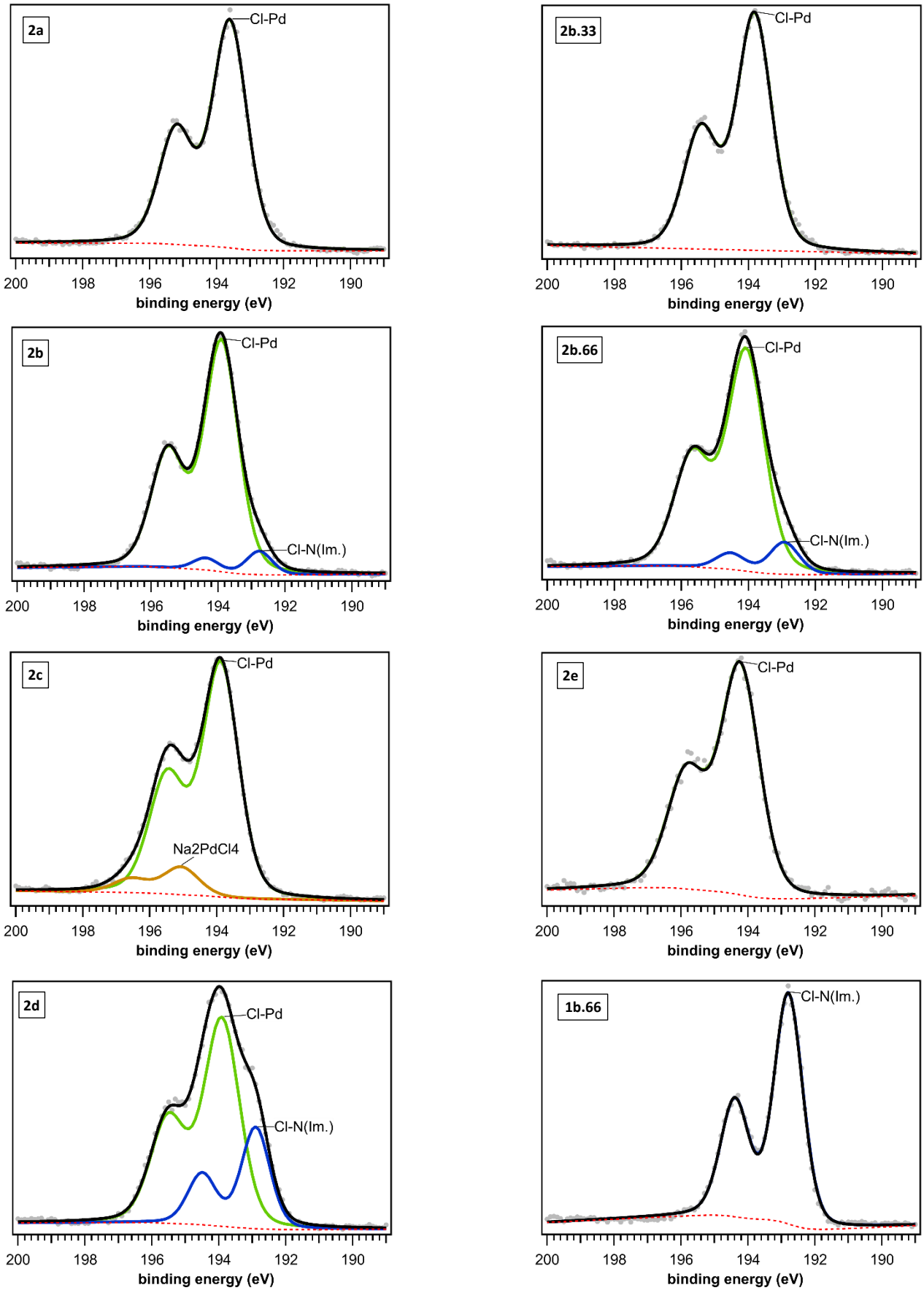

Figure S31 Cl 2p core level XPS spectra of precatalysts **2a-e** and polymer **1b.66**.

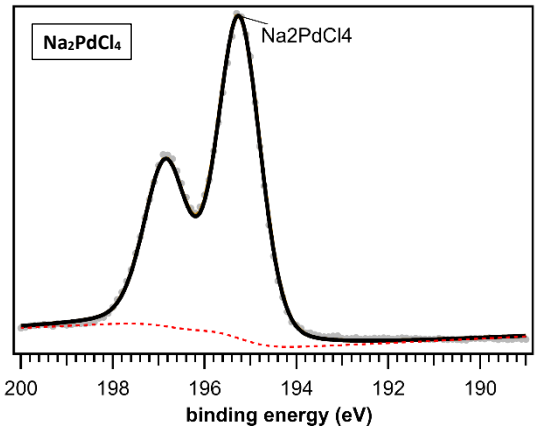

Figure S32 Cl 2p core level XPS spectrum of Na_2PdCl_4.

Table S8 Cl 2p binding energies with relative abundance of each species for precatalysts **2a-e** and polymer **1b.66**, where Cl-$N_{(Im.)}$ shows chlorine associated with imidazolium nitrogen atoms.

Sample	Cl-Pd	Cl-$N_{(Im.)}$	Na_2PdCl_4	Cl-Pd	Cl-$N_{(Im.)}$	Na_2PdCl_4
	$2p_{3/2}$	$2p_{3/2}$	$2p_{3/2}$	%	%	%
2a	193.6			100		
2b	193.9	192.8		93	7	
2c	193.9		195.1	90		10
2d	193.9	192.9		72	28	
2b.33	193.8			100		
2b.66	194.1	192.9		90	10	
2e	194.2			100		
1b.66		192.8			100	
Na_2PdCl_4			195.3			100

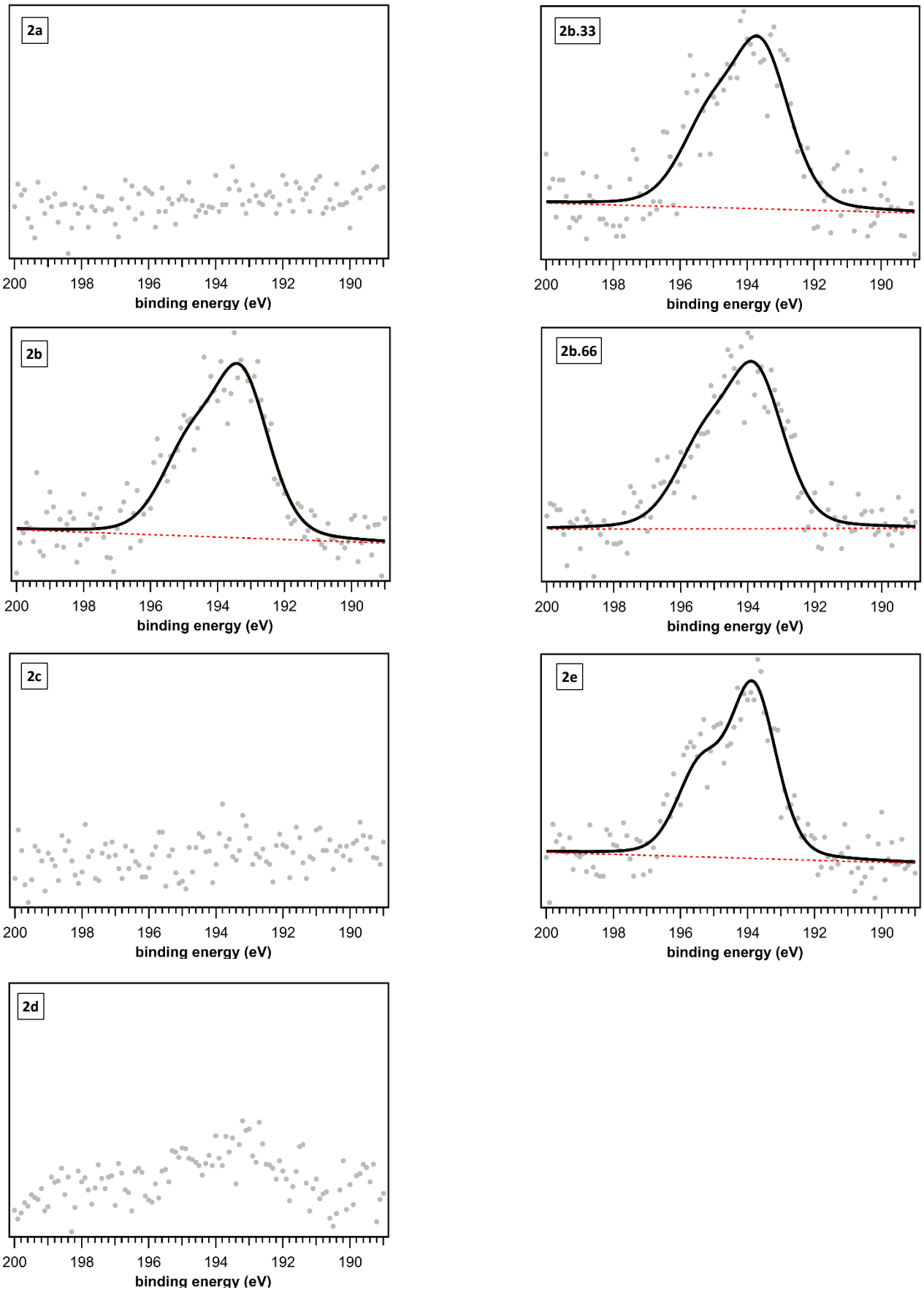

Figure S33 Cl 2p core level XPS spectra of catalysts generated from precatalysts **2a-e** after 2 hours of hydrogenation.

Table S9 Cl 2p binding energies for catalysts generated from precatalysts **2a-e** after 2 hours of hydrogenation.

Sample	**P1**
	$2p_{3/2}$
2a NP	-
2b NP	193.3
2c NP	-
2d NP	193.1
2b.33 NP	193.6
2b.66 NP	193.8
2e NP	193.8

The relative intensity of chlorine signals was greatly reduced after catalysis which is unsurprising as $PdCl_4$ is reduced to metallic Pd, and any imidazolium associated chloride is lost due to cleavage of the benzylic imidazolium group. As a consequence of this, the signal to noise ratio of spectra is quite poor and some fittings (namely **2d** and **2b.33**) should be treat with caution.

References

1. S. Doherty, J. G. Knight, T. Backhouse, E. Abood, H. Al-shaikh, A. R. Clemmet, J. R. Ellison, R. A. Bourne, T. W. Chamberlain, R. Stones, N. J. Warren, I. J. S. Fairlamb and K. R. J. Lovelock, *Adv. Synth. Catal.*, 2018, **360**, 3716–3731.
2. K. N. Wood and G. Teeter, *ACS Appl. Energy Mater.*, 2018, **1**, 4493–4504.
3. M. Schmid, H. P. Steinrück and J. M. Gottfried, *Surf. Interface Anal.*, 2014, **46**, 505–511.
4. Y. Zhang, Y. Cai, Y. Guo, H. Wang, L. Wang, Y. Lou, Y. Guo, G. Lu and Y. Wang, *Catal. Sci. Technol.*, 2014, **4**, 3973–3980.